universität wien

MASTERARBEIT

Titel der Masterarbeit

„Molecular Mechanisms of Cargo Selection in Cytoplasm-to-Vacuole Targeting“

Verfasserin

Christine Isabel Abert, BSc

angestrebter akademischer Grad

Master of Science (MSc)

Wien, 2013

Studienkennzahl lt. Studienblatt:	A 0669834
Studienrichtung lt. Studienblatt:	Masterstudium Molekulare Biologie
Betreuerin / Betreuer:	Dr. Sascha Martens

Abstract

Autophagy is a degradation process conserved in eukaryotes. During autophagy, a membrane structure called isolation membrane is formed *de novo* that engulfs cytoplasmic cargo gradually and eventually forms a double membrane-bound vesicle called autophagosome. This 140-900 nm vesicle is transported to the vacuole in yeast or the lysosome in higher eukaryotes. There its outer membrane fuses with the membrane and its inner membrane and its contents are degraded. When cells face lack of nutrients, autophagic break down of macromolecules is elicited in order to recycle material for anabolic metabolism. But autophagy can also target selected cargoes independently of the nutritional state of a cell. One example of selective autophagy is the cytoplasm-to-vacuole targeting (Cvt) pathway in *Saccharomyces cervisiae*. Here, several specific cargoes are brought to the vacuole in a constitutive manner. It is important for the cell to ensure that only the correct cargo, one of which is the vacuolar protease Ape1, is engulfed by the autophagic membrane. Otherwise there would be a waste of energy in form of a constant loss of functional cellular factors to vacuolar degradation. Responsible for specific protein transport to the vacuole is the Cvt receptor molecule Atg19, the ubiquitin-like molecule Atg8 on the autophagic membrane and the Cvt cargo prApe1, the inactive precursor of vacuolar Ape1. The interaction of these factors confers selectivity during Cvt. This thesis aimed to elucidate the molecular mechanisms underlying these interactions applying several *in vitro* experimental set-ups.

Zusammenfassung

Autophagie ist ein Degradationsweg, der in allen Eukaryoten vorkommt. Im Verlauf des Proteinabbaus durch Autophagie wird eine Membranstruktur, die sogenannte Isolationsmembran, *de novo* gebildet, welche zytoplasmatische Cargo umschließt und schließlich ein doppelmembranständiges Autophagosom bildet. Das so entstandene Autophagosom misst zwischen 140 und 900 nm im Durchmesser. Es wird entweder zur Vakuole (in Hefen) oder zum Lysosom (in höheren Eukaryoten) transportiert, wo die äußere Membran mit dem Organell fusioniert um den inneren Vesikel zu entlassen. Nach Zersetzung der inneren Membran wird der Inhalt des Vesikels proteolytisch aufbereitet. Im Falle von Nährstoffmangel wird Autophagie in Gang gesetzt und so Makromoleküle in ihre Bausteine zu spalten, die dann weiterhin einen funktionellen anabolischen Metabolismus gewährleisten. Allerdings können auch gezielt unabhängig von Nährstoffverfügbarkeit bestimmte Substanzen durch Autophagie prozessiert werden. Ein Beispiel hierfür stellt der sogenannte cytoplasm-to-vacuole targeting pathway in *Saccharomyces cervisiae* dar. Mehrere Proteine werden hier spezifisch und konstitutiv zur Vakuole transportiert. Während dieses Prozesses ist es von essentieller Bedeutung, dass nur die ausgewählten Proteine, z. B. die Hydrolase prApe1, von der Membran umschlossen werden, um einen kontinuierlichen Energieverlust durch Abbau von funkionellem zytoplasmatischem Material zu vermeiden. Verantwortlich für diesen spezifischen Proteintransport sind der Cvt-Rezeptor Atg19, das membranständige Protein Atg8, das strukturelle Ähnlichkeit mit Ubiquitin aufweist und das zu transportierende Protein prApe1 (die inaktive Vorform des Enzyms Ape1). Die Interaktion dieser Faktoren garantiert Selektivität des Cvt pathways. Im Zuge dieser Arbeit sollen die molekularen Mechanismen, die diesen Interaktionen zu Grunde liegen, durch verschiedene Experimente aufgezeigt werden.

I Introduction

Autophagy is an alternative degradation process in eukaryotic cells. It has been shown to be involved in various pathologies like bacterial infection[1,2], neurodegenerative diseases[3] and cancer[4,5]. In contrast to the proteasomal degradation pathway, where a cytosolic protein complex is responsible for the break-down of specific polypeptides[6], autophagy delivers cytoplasmic material to the lytic compartment (the vacuole in yeast or the lysosome in higher eukaryotes). Autophagy occurs in three mechanistically different ways[7]. These are microautophagy[8,9], chaperone-mediated autophagy[10] and macroautophagy[11]. During microautophagy a vesicle containing cytoplasmic material buds into the vacuole or the lysosome and is pinched off in order to be broken down within the organelle. In chaperone-mediated autophagy, proteins destined for the lytic compartment are kept in an unfolded state in the cytosol and are delivered to the vacuole/lysosome via specific transport proteins. The third and best-studied autophagic process is termed macroautophagy (referred to as autophagy in the following)[12-14], where cytoplasmic material is engulfed by a *de-novo* formed double membrane (*isolation membrane* or *phagophore*). The generated 300-900 nm vesicle is termed an autophagosome[15]. It is brought to the vacuole/lysosome. After fusion of the outer membrane of the autophagosome with the vacuole/lysosome, the resulting autophagic body is broken down and its contents are degraded (see Figure 1).

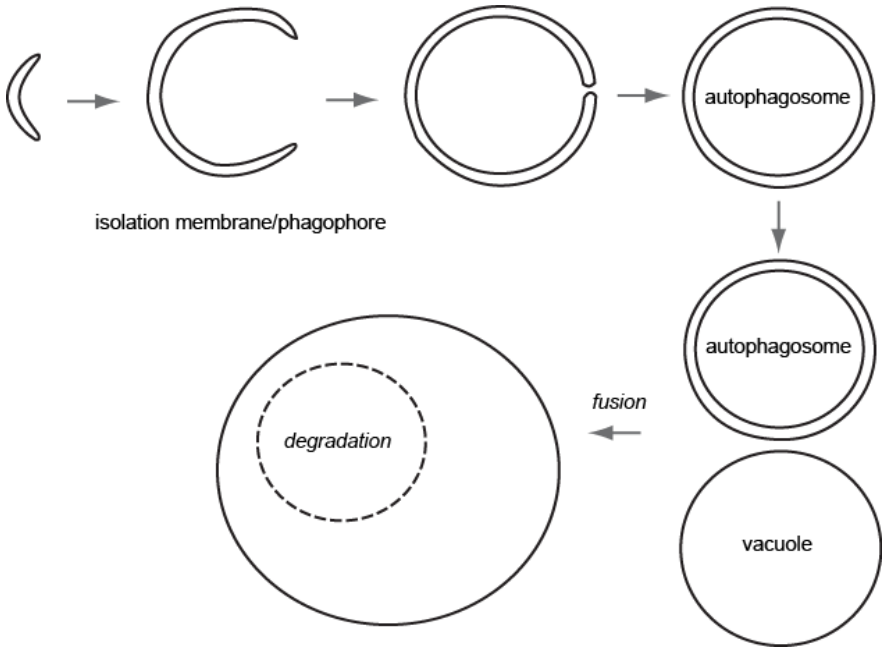

Figure 1: Several steps are required for degradation by autophagy
During autophagy, a membrane structure is formed *de novo.* This so-called isolation membrane or phagophore engulfs cytoplasmic material and finally encloses it. The resulting autophagosome is transported to the lytic compartment (the vacuole in yeast). After fusion with the vacuole, the contents of the autophagosome are degraded within the organell.

Microautophagy and macroautophagy are generally regarded as degradation pathways for recycling cytoplasmic macromolecules and thus providing building blocks for anabolic processes. This is extremely important when the cell has to cope with nutrient deprivation, for example during the neonatal starvation period. Mice deficient in Atg5, an essential autophagy factor, show no evident defects after birth but die within days of starvation. Since immediately after birth no food is taken up, nutrients have to be recycled within the body, which happens via autophagy[16]. In yeast, autophagy of random cytoplasm can be elicited by growth in medium lacking a nitrogen source. Notably, autophagic pathways can be triggered by a lack of nutrients but also occur constitutively independent of the metabolic state of a cell[17]. Whereas autophagy of random cytoplasm is induced by nutrient limitation, constitutive autophagic pathways (i.e. independent of general nutrient availability) target to a specific cargo. Either event leads to induction of a signaling cascade involving the target-of-rapamycin kinase complex 1(TORC1)[18]. If TORC1's kinase activity is inhibited by starvation or treatment with the drug rapamycin autophagy will be induced[19].

Several proteins -most of them termed *Au*tophagy related *g*ene products or *Atg*s[20]-are essential for autophagosome formation. The Atg1 kinase complex, comprising Atg1/ULK1 in yeast and mammalian cells respectively, Atg13 and additional Atgs, depending on the type of autophagy[21], is the most upstream factor after the TOR complex[18,22]. Its assembly as well as its kinase activity increases upon autophagy induction. Several Atg proteins have been shown to be phosphorylated by the Atg1 kinase complex, like Atg13 and mammalian FIP200, which are part of the complex themselves[23].

The phosphatidylinositol-III-kinase-complex consisting of the central PI-III kinase Vps34 (Vacuolar Protein Sorting 34) and Atg6/Beclin-1, Atg14 and Vps15/p115in yeast and mammals respectively converts phosphatidylinositol (PI) to phosphatidylinositol-3-phosphate (PI3P), which plays a role in autophagosome formation probably by the recruitment of several autophagic proteins to the membrane[24].

Atg9 is the only transmembrane protein amongst the Atgs. It has been shown to localize to vesicles and to cycle between the site of autophagosome formation and peripheral sites. Its knockout leads to defects in autophagy[25,26] but the mechanistic bases of this defect is not fully understood. Atg9 vesicles might help to deliver membrane material as well as other factors to the expanding phagophore.

Two ubiquitination-like conjugation systems are involved in autophagy. These are the Atg8 and Atg12 conjugation systems[27]. In the Atg12 conjugation system the ubiquitin-like molecule Atg12 is conjugated to Atg5 through the action of the E1-like activating enzyme

Atg7 and the E2-like enzyme Atg10. This conjugation process resembles ubiquitination as Atg7 forms a thioester with the reduced Sulfur-group of Atg12 and then passes Atg12 on to Atg10 from where it is covalently attached to an internal lysine of Atg5[28].Subsequently, the Atg12–Atg5 conjugate binds to Atg16 to form the Atg12–Atg5-Atg16 complex. The complex localizes to isolation membranes but dissociates before autophagosome completion[28].

In the Atg8 conjugation system Atg8 becomes covalently attached to the head-group of the membrane lipid phosphatidylethanolamine (PE). The first step of the conjugation reaction is carried out by the protease Atg4 that in the case of *S. cervisiae* cleaves Atg8's C-terminal arginine in order to expose a glycine residue[27]. Subsequently the E1-like enzyme Atg7 and the E2-like enzyme Atg3 conjugate Atg8 to PE on the isolation membrane[29]. The Atg12–Atg5-Atg16 complex facilitates Atg8-PE conjugation by acting in an E3-like manner[16]. There is one Atg8 in *S. cervisiae*, but several homologues have been found in higher eukaryotes, like GABARAP, LC3 and GATE-16 in mammals[30]. The x-ray structure of yeast Atg8 and several homologues (p. ex. five human Atg8 homologues) has been resolved[31-35]. In addition to an ubiquitin-like core, Atg8-family proteins have two N-terminal α-helices, α1 and α2. α2 forms together with a β strand (β2) a hydrophobic pocket that is involved in binding of autophagy-receptor molecules like Atg19[36]. A specific sequence in the receptor molecule called LIR (*L*C3-*I*nteracting-*R*egion) is responsible for binding to Atg8 (see Figure 2)[36,37].

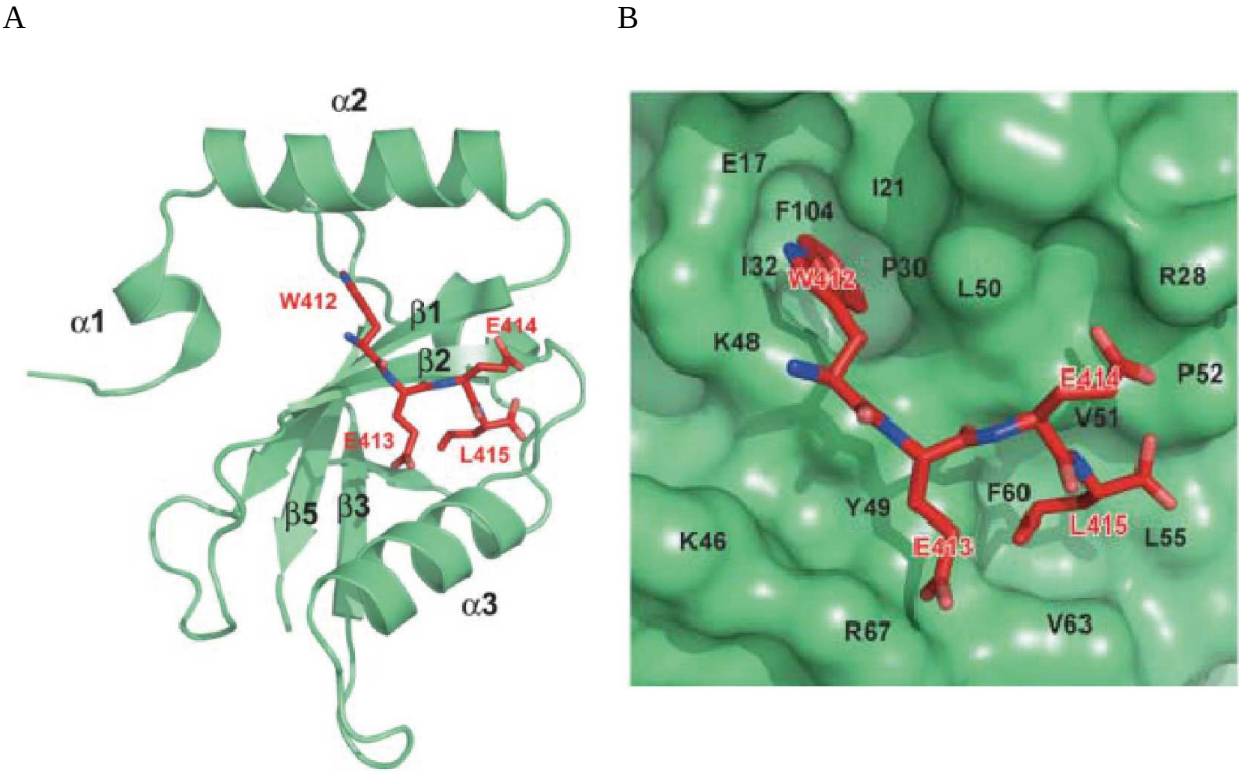

Figure 2: Crystal structure of Atg19's LIR motif binding to Atg8 resolved
Atg8 in green ribbon (A) and surface (B) models, Atg19's LIR peptide (WEEL) in red stick model.Atg19's tryptophan is shown to poke into a hydrophobic pocket in Atg8 at the interface of the N-terminal α2 helix and the β2-strand of the ubiquitin-like core of the molecule. Taken from Noda *et al.*, 2008[36].

Apart from bulk autophagy, there are several selective autophagic pathways that recognize specific cargo[13,38,39]. These mediate, for example clearance of intracellular pathogens like *Salmonella typhimurium*[1] or *Shigella flexneri*[2] or selective degradation of potentially toxic protein aggregates like alpha-synuclein in Parkinson's disease[40,41] or neurofibrillar tangles (tau-aggregates) in Alzheimer's disease[42]. Also cell organelles, like mitochondria[43] and peroxisomes[44,45], parts of the ER[46] and the nucleus[47] as well as RNA-containing and stress granules[48] have been shown to be degraded by selective autophagy. Interestingly, selective autophagy can also serve as a biosynthetic pathway as is the case in cytoplasm to vacuole targeting (Cvt) in *Saccharomyces cervisiae*[38]. Here, cargoes are the inactive cytosolic precursors of the vacuolar enzymes Ape1 (aminopeptidase 1) and Ams1 (alpha-mannosidase 1)[37], furthermore the enzymes Ape4[49]and Ty1 retrotransposon particles[50]. After autophagic delivery to the vacuole, Ape1 is proteolytically activated and executes its enzyme function in this compartment[14]. Selectivity for these cargoes is conferred by the receptor, Atg19 (prApe1, Ams1)[37] or Atg34 (Ams1)[51] by binding to the cargo[37]. Atg19 contains interaction sites for prApe1 (coiled coil domain in the N-terminal half of the protein) and Ams1 (atypical immunoglobin-like β-sandwich fold[52]), whereas Atg34 only binds Ams1 via a structurally

similar binding site as Atg19[52]). Atg34 only has one Atg8 binding site at its very C-terminus[52], whereas Atg19 seems to have several. Interestingly, in contrast to Atg19 Atg34 is dispensable for maturation of prApe1, i.e. for functional Cvt[51]. Atg34 selectively binds to its cargo as well as Atg8 and Atg11 during autophagy, but it does not confer exclusive transport of its cargo as opposed to Atg19. Atg34 brings the cargo to the forming autophagosomal membrane but does not bind tightly to the membrane or even closely wrap it around the cargo, as is the case for Atg19 and the Cvt-vesicle. Another interaction of the receptors required for selective types of autophagy is binding of the scaffold protein Atg11[53] in that it brings the complex to the PAS[54]. Finally binding of the autophagic membrane via interaction with lipidated Atg8[36,55] is indispensable for formation of the autophagic vesicle (see scheme Figure 3).

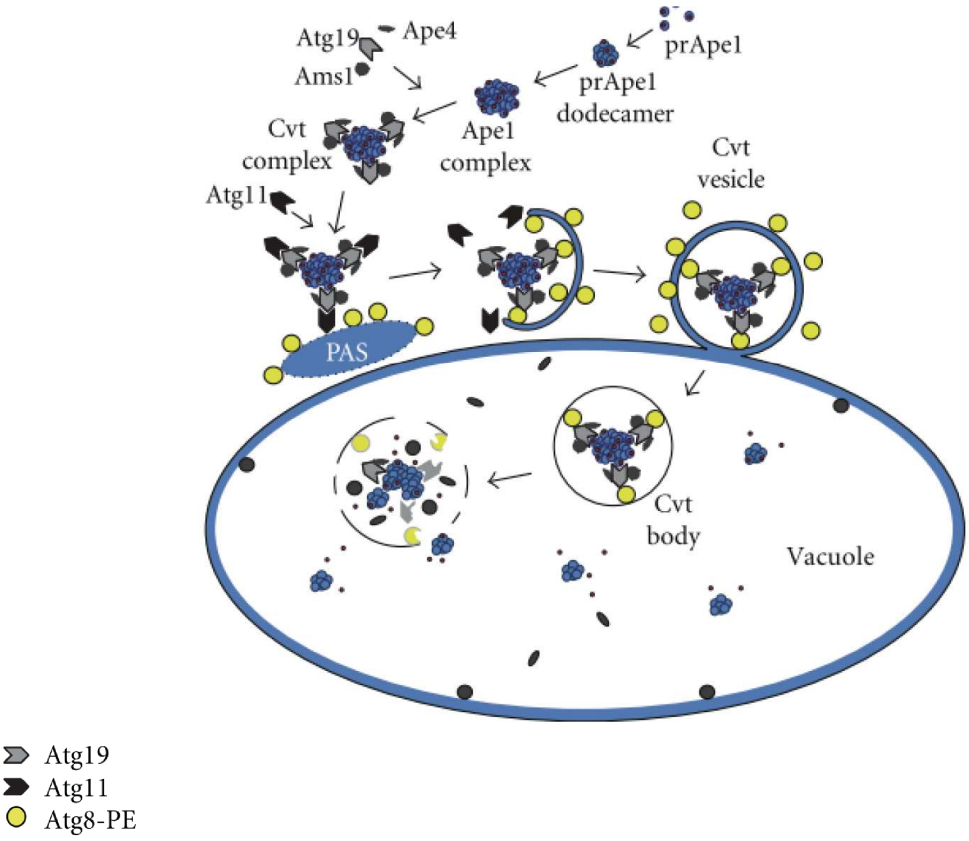

Figure 3: Atg19 interacts with several proteins during Cvt
After prApe1 aggregation in the cytosol, Atg19 binds to this complex. Additional cargoes are the vacuolar hydrolyses Ams1 and Ape4. These associate as well forming the Cvt-complex, which interacts with Atg11 and is brought to the PAS. The Cvt-complex is enwrapped by the Cvt membrane after binding PE-conjugated Atg8. Taken from Umekawa and Klionsky, 2012[56].

The precursor form of Ape1, referred to as prApe1 contains a 45 amino acids long N-terminal propeptide sequence and resides in the cytoplasm. prApe1 is assumed to form trimers, which assemble first into hexameres and then into dodecameres to finally form higher aggregates.

This assembly is mediated by Ape1's propeptide which is thought to protrude from the surface of the higher oligomeres[57,58]. The prApe1 aggregates are recognized by the autophagic receptor Atg19. GFP-Atg19 has been shown to localize to prApe1 and Atg11 positive punctae in *S. cerevisiae.* in starvation (synthetic minimal medium with glucose as carbon source lacking a nitrogen source, SD-N) as well as in growth (SMD) conditions. An Atg19 deletion strain is defective in Ape1 processing i.e. lacks detectable amounts of the mature vacuolar form of Ape1. However, Atg19 deletion cells don't show defects in general bulk autophagy as assessed by the detection of free GFP in GFP-Atg8 expressing cells [59,60]. This indicates that prApe1 is specifically transported to the vacuole in growing conditions, i.e. constitutively, but can also use starvation-induced bulk autophagy to serve its function in the lytic compartment. Autophagy receptors have several interaction sites for different proteins. In the case of Atg19, a central coiled-coil domain (aa 124-254) is responsible for binding the prApe1 cargo[59]. Atg11, which is a scaffold protein required for all types of selective autophagy in yeast[53], interacts with a C-terminal motif of Atg19[54]. Binding of Atg8 by Atg19 has been shown to depend on a so called *L*C3-*I*nteracting-*R*egion or LIR motif at the very C-terminus of Atg19[37,61]. This motif has been shown to be essential for a functioning Cvt pathway. When W412 of Atg19's C-terminal LIR WEEL is mutated to A in yeast, detected amounts of mature Ape1, the active vacuolar form of prApe1, are severely decreased. Mutating L415 of the LIR to A results in a similar, but less drastic effect. Introduction of both mutations suppresses Cvt almost completely, mApe1 is detected barely above background levels[61]. Classical LIR-motifs consist of a WxxL motif (tryptophan, any two amino acids, leucine) which binds in the ubiquitin-like fold of Atg8 (or -homologues). The bulky shapes as well as the hydrophobicity of tryptophan and leucine ensure a selective interaction by pointing into two hydrophobic pockets in Atg8 respectively (see Figure 2). LIR motifs and variations thereof have been discovered in several yeast and mammalian autophagy receptors[39], such as Atg30 and Atg32 (required for yeast pexophagy[44,45] and mitophagy[43] respectively) or p62 (clearance of ubiquitinated protein aggregates or pathogens in mammalian cells)[62]. There are also LIR motifs that do not strictly contain an initial W and a L in the end, for example the FVEI motif in optineurin, a xenophagy-receptor in mammals[63] or the LVV motif in the mammalian receptor NDP52 (xenophagy[64], mRNA-processing: dicer-clearance[65]) required for specific interaction with one Atg8 homologue (LC3C)[64,66]. LIRs are of crucial importance for selective incorporation of the cargo into autophagic vesicles because they enable the receptor to link the cargo to Atg8-coated isolation membranes. For the Cvt-specific autophagic vesicles the double membrane is wrapped around the cargo in a tight manner, thus not only selectively

transporting it but at the same time excluding other cytoplasmic material (see Figure 3 and Figure 4 (B)).

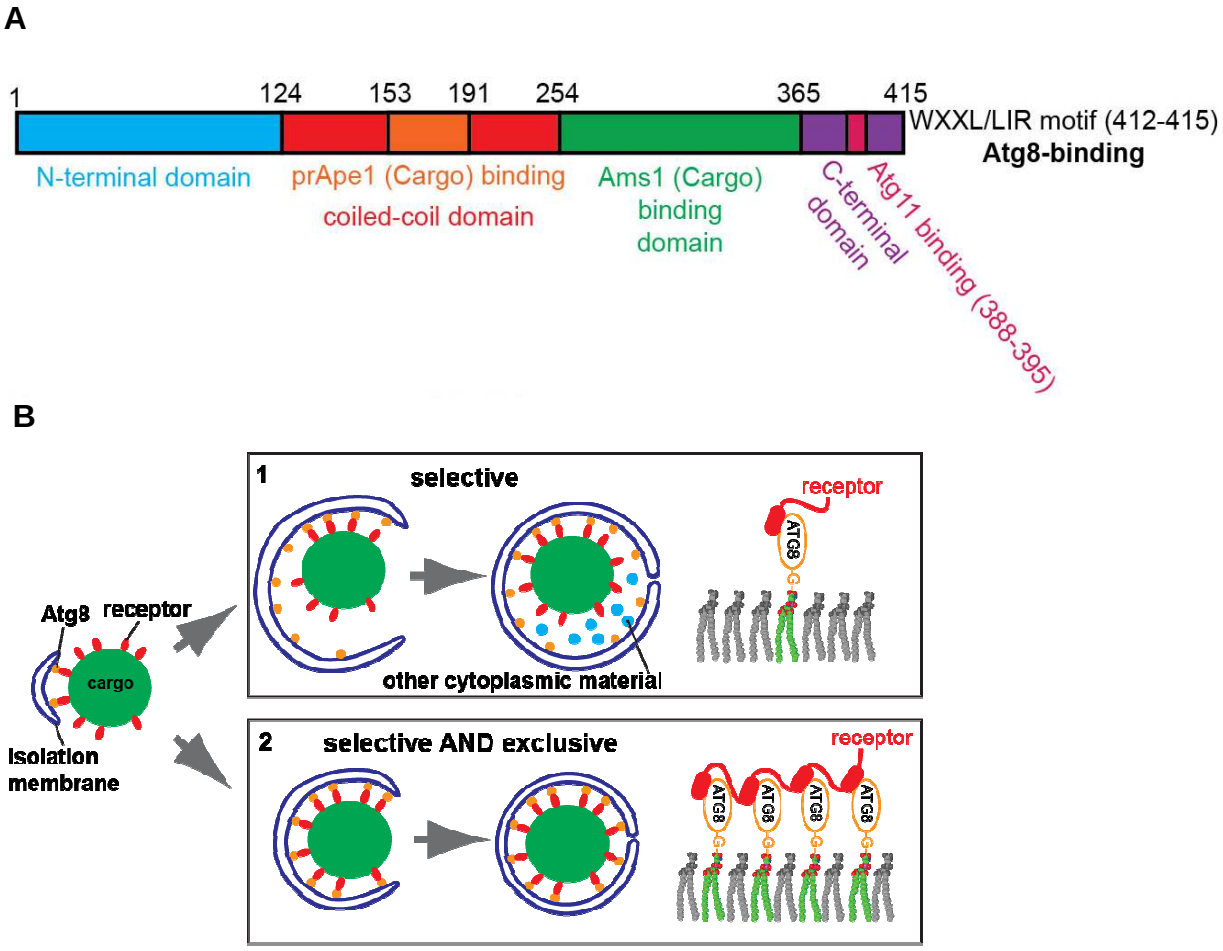

Figure 4: Domain organization and function of the receptor Atg19 in the Cytoplasm-to-Vacuole Targeting pathway
Domains are shown in different colors, amino acid number on top.(B) Autophagy receptors mediate selectivity by binding to selectivity by binding to the cargo and to lipidated Atg8 on autophagic membranes. Atg34 has one Atg8 binding site and confers selective autophagic transport of its cargo but does not exclude other cytoplasmic material (upper panel). Several binding sites in Atg19 for Atg8 ensure tight interaction and thus selective and exclusive enclosure of the cargo into the Cvt vesicle (lower panel).

Several experiments conducted prior to this thesis indicated that there might be more complex aspects to be considered in Atg8-Atg19 interaction than previously assumed (personal communication J. Sawa-Makarska, S. Martens). Notably, several results suggest that there is at least one more Atg8 binding site in Atg19 apart from for the well-characterized classical LIR motif (WEEL, amino acids 412-415). In size exclusion chromatography (SEC) as well as affinity-pull down experiments using mutant forms of Atg19 where the LIR-dependent Atg8-binding was abolished either by the W412A point mutation[61] or truncation of the entire LIR (Atg19 aa1-407), residual binding of Atg8 was still observed. Furthermore it seemed that increasing the concentration of Atg19 in these experiments enhances the interaction with Atg8. The same was observed when only the C-terminal domain of Atg19 (aa365-415) was

used. Apparently also the Cvt cargo prApe1 has an influence on the Atg19-Atg8 interaction. In particular, addition of the 45aa N-terminal propeptide of Ape1 lead to an increase in Atg19-Atg8 binding in pull down experiments suggesting that the Cvt cargo is a major determinant in receptor-Atg8 binding. All these observations provide strong evidence for the existence of several Atg8 binding sites in the cargo receptor Atg19. These could reside in the C-terminal domain of the protein. Furthermore, they might be activated by binding the prApe1 cargo by Atg19 possibly by releasing a structural self-inhibition of the receptor that exposes the additional interaction sites and renders them accessible for binding.

The aim of this thesis was to further elucidate the molecular mechanisms underlying the Atg8-Atg19 interaction focusing on the identification of the canonical LIR-independent Atg8 interaction sites in Atg19. To this end recombinantly expressed and purified Atg8 and Atg19 were studied in various experimental set ups including pull down experiments, size exclusion chromatography and reconstitution systems employing giant unilamellar vesicles.

II Methods

SDS-PAGE

Protein samples for sodium-dodecylsulfatepolyacrylamid gel electrophoresis (SDS-PAGE) were diluted in loading buffer containing 375 µM Tris-Cl pH 6.8, 12% SDS (AppliChem, Darmstadt, Germany, VWR, PA, USA), 60% glycerol (Sigma-Aldrich, MO, USA), 0.6 % bromphenolblue (both Merck, NJ, USA) and β-mercaptoethanole (both Merck, NJ, USA) and boiled at 100°C for 30 sec to 5 min. Samples were loaded on 10-20% polyacrylamide (Roth, Karlsruhe, Germany) gels (containing TEMED (Sigma-Aldrich), 10% APS) depending on their known or estimated molecular weight (predicted *in silico* by the ProtParam tool, http://web.expasy.org/protparam/). Gels were run at a fixed voltage of 100 – 300 V for 20 – 60 min using a Power Pac Basic power supply (Bio Rad, CA, USA). Proteins were detected by boiling and 15 min incubation in coomassie brilliant blue and subsequent destaining in 40 % EtOH and 10 % acetic acid (AppliChem). PageRulerPrestained Protein Ladder (Thermo Scientific, MA, USA) was used to determine the running height of a protein in SDS-Page.

Western Blot

After separation by SDS-PAGE protein samples were transferred to nitrocellulose membranes (GE Healthcare). Uniform protein loading and transfer were verified by Ponceau (0.1 % in 5 % acetic acid) staining. Membranes were blocked in Tris buffered saline with 0.1% Tween 100 (Sigma, TBST) containing 3% non-fat dry milk powder (Roth) for 1 h. Western blots were probed with primary antibodies for 1 h at room temperature (GST-Atg8 antibody from serum (kind gift from C. Kraft) or over night at 4°C (anti-Penta-His-antibody (Qiagen, Venlo, Netherlands)), washed three times with TBST, and then incubated with the appropriate secondary antibodies (Jackson ImmunoResearch, PA, USA) for 2 h. Membranes were then washed with TBST three times, before developing with homemade (100 mMTris pH 8.5,) or Pico (ThermoScientific) enhanced chemoluminescent substrate. Films (ThermoScientific) were developed for 1s to 20 minutes in a Curix 60 developing machine (Agfa, Mortsel, Belgium).

Cloning strategy

Recombinant plasmids for protein expression were generated by polymerase chain reaction in an EppendorfMastercycycler Gradient PCR machine using the respective oligonucleotides as primers (see Table 1, Sigma-Aldrich). The PCR product and the over expression plasmid

(pGEX4-T-1 (GE Healthcare) for GST-fusion-proteins or pEtDuet- (Novagen, MA, USA) for 6xHis-tagged proteins) were cut for 2 h at 37° with the appropriate restriction enzymes (New England Biolabs, MA, USA). After controlling the size and amount of the generated DNA by electrophoresis at 140 V on a Power Source power supply (VWR) on 1-2% agarose (FMC Bioproducts, ME, USA) substituted with SYBRSafe DNA gel stain (Invitrogen (Life Technologies Ltd.), Paisley, UK), products were purified using a PCR-/gel purification kit (SLG). The digested PCR products were ligated into the desired plasmid for 20 min at room temperature using T4-ligase and the respective buffer (New England Biolabs). The recombinant plasmids were amplified in DHα5 cells and purified using a plasmid mini preparation kit (ThermoScientific).

Sequence 5'-3'	**Purpose, introduced restriction sites**
CCCCCCCCCGAATTCATGAACAACTCAAAGACTAACC	forward primer for Atg19 amplification & cloning into pGEX-4-T1, EcoRI-site
CCCCCCCCCGTCGACCTAGAGTTCTTCCCAAGTCAG	reverse primer for Atg19 amplification & cloning into pGEX-4-T1, SalI-site
GAAAAAGCCCTGACTGCGGAAGAACTCTAGGTC	forward primer to introduce W412A mutation into Atg19
GACCTAGAGTTCTTCCGCAGTCAGGGCTTTTTC	reverse primer to introduce W412A mutation into Atg19
GCATCCCAAGAGCCAGCTTACTCCTTTCAAATC	forward primer to introduce F376A mutation into Atg19
GATTTGAAAGGAGTAAGCTGGCTCTTGGGATGC	reverse primer to introduce F376A mutation into Atg19
AGAGCCATTTTACTCCGCTCAAATCGATACGTTA	forward primer to introduce F379A mutation into Atg19
TAACGTATCGATTTGAGCGGAGTAAAATGGCTCT	reverse primer to introduce F379A mutation into Atg19
CAAATCGATACGTTAGCAGAACTGGATGACTCT	forward primer to introduce P385A mutation into Atg19
AGAGTCATCCAGTTCTGCTAACGTATCGATTTG	reverse primer to introduce P385A mutation into Atg19
ATCGATACGTTACCAGCACTGGATGACTCTAGT	forward primer to introduce E386A mutation into Atg19
ACTAGAGTCATCCAGTGCTGGTAACGTATCGAT	reverse primer to introduce E386A mutation into Atg19
ATTAACTTAAGGCCACCTCTCGAGTCAAGATTATCTGCAGAA	forward primer to create Atg19-Atg34 chimera by insertion of XhoI sits (after Pro c-terminally of Atg19's ABD)
TTCTGCAGATAATCTTGACTCGAGAGGTGGCCTTAAGTTAAT	reverse primer to create Atg19-Atg34 chimera by insertion of XhoI sits (after Pro c-terminally of Atg19's ABD)
ATAACTCTAAAATCTCCACTCGAGCTAGCCTCATTTTCGACA	forward primer to create Atg19-Atg34 chimera by insertion of XhoI sits (after Pro c-terminally of Atg19's ABD)
TGTCGAAAATGAGGCTAGCTCGAGTGGAGATTTTAGAGTTAT	reverse primer to create Atg19-Atg34 chimera by insertion of XhoI sits (after Pro c-terminally of Atg19's ABD)

CCCCCCCCGAATTCTCTGCAGAAAGTTTACAGGC	forward primer for Atg19 aa(365-415) amplification, EcoRI-site
CCCCCCGTCGACCTATTCATTGTCGTCACCGTCATA	reverse primer to truncate aa 408-415 from Atg19
CCCCCCCGTCGACCTACTCTTGGGATGCCTGTAA	reverse primer to truncate aa 375-415 from Atg19
CCCCCCCGTCGACCTATAACGTATCGATTTGAAAGGA	reverse primer to truncate aa 385-415 from Atg19
CCCCCCCGTCGACCTAGGATGTACTGATGATACTAGAGTC	reverse primer to truncate aa 397-415 from Atg19
CCCCCCCGAATTCTTTTACTCCTTTCAAATCGATAC	forward primer to truncate aa 1-375 from Atg19 W412A
CCCCCCCGAATTCGAACTGGATGACTCTAGTATC	forward primer to truncate aa 1-385 from Atg19 W412A
CCCCCGAATTCTCACTCTCTTATGACGGTGACGACAATGAAAAAGCCCTGACTGCGGAAGAACTCTAGGTCGACCCCCC	Forward primer to synthesize Atg19 W412A aa 1-398
CCCCCCCGTCGACCTATTCCTTCTCCTCGGAGGGC	reverse primer for Atg19 aa(1-123) amplification, SalI-site
CCCCCCCCGAATTCGTGGAACCCCCAAATGAGC	forward primer for Atg19 (124-254) amplification ,EcoRI-site
CCCCCCCCGAATTCGTGGAACCCCCAAATGAGC	reverese primer for Atg19 (124-254) amplification , SalI-site
CCCCCCCCGGATCCATGGAGGAACAACGTGAAATAC	forward primer for prApe1 aa(1-45) amplification in pGEX-4-T1, BamHI-site
CCCCCCCCGTCGACTCACGAGGATGCACCACGAATTTTC	reverse primer for prApe1 aa(1-45) amplification in pGEX-4-T1, SalI-site
CCCCCCCCGTCGACGATGGAGGAACAACGTGAAATAC	forward primer for prApe1 aa(1-45) amplification & cloning into pmCherry-N1 or pmEGPF-N1, SalI
CCCCCCCCGGATCCACGAGGATGCACCACGAATTTTC	reverse primer for prApe1 aa(1-45) amplification & cloning into pmCherry-N1 or pmEGPF-N1, BamHI
CCCCCCCCCGGATCCGGAAAACCTGTATTTTCAGGGAATGAAGTCTACATTTAAGTCTG	forward primer for Atg8 amplification & cloning into pEtDuet, BamHI-site
CCCCCCCCCGCGGCCGCCTAGCCAAATGTATTTTCTCCTGAG	reverse primer for Atg8 amplification & cloning into pEtDuet, NotI-site

Table 1: Oligonucleotides used for this thesis

Protein purification

Proteins were expressed in Rosetta pLysS cells (EMD Millipore) for 3 h at 37°C (6xHis-tagged Atg8) or at 18°C over night. Cells were induced with 0.5 mM IPTG (only His-tagged Atg8) or 0.1 mM IPTG (isopropyl-β-D-thiogalactopyranosid, Peqlab). The cells were pelleted at 4000 rpm and 4°C for 15 min. Pellets were resuspended in cold lysis buffer containing 50 mM HEPES pH 7.5, 300 mM NaCl, 1 mM $MgSO_4$, 1% Pefablock (Roth), DNase (Fluka (Sigma-Aldrich)) and 2 mM β-mercaptoethanole. After flash freezing in liquid nitrogen and

thawing, cells were lysed by 30 sec sonication at 73 D and cycle 40. Lysates were cleared by ultracentrifugation at 4°C and 41000 rpm for 45 min.

Purification of GST-fusion proteins

Soluble fractions of cell lysates were bound to 5 to 10 ml glutathione-coupled sepharose beads (GE Healthcare) rolling at 4°C for 1 h. The beads were washed 5x for 10 min in a wash buffer containing 50 mM HEPES pH 7.5, 300 mM NaCl and 1 mM DTT and spun down at 4000 rpm for 5 min. Unspecific ionic interactions were disrupted by washing in 700 mM NaCl buffer for 30 min. After two 10 min washes in 300 mM NaCl, the GST-fusion proteins were eluted from the beads in a 1:1 ratio of beads to wash buffer substituted with 40 mM reduced glutathione (Sigma-Aldrich) at pH 8 for 2 h at room temperature. The beads were washed 3x in glutathione buffer and all supernatants were pooled.

To remove the GST-tag from the expressed proteins, lyophilized thrombine (Serva, Heidelberg, Germany) dissolved in 1 ml wash buffer was added to the beads containing the GST-fused proteins. The GST-tag was cleaved off by the protease leaving the beads rolling either for 1-2 h at room temperature or over night at 4°C. Beads were then washed 3x in wash buffer and all supernatants were pooled, concentrated and subjected to size exclusion chromatography. The protein fractions were checked in SDS-PAGE before concentrating in appropriate cut-out filters (EMD Millipore, MA, USA) and flash freezing in liquid nitrogen. Proteins were stored at -80°C.

Purification of His-tagged proteins

Cleared lysates of expressed His-tagged proteins were filtered through 0.45 um cut-out filters and subjected to His-trap elution using 10 – 300 mM imidazole on an Äkta Purifier FPLC system. After protein was detected on SDS-PAGE corresponding fractions were pooled and concentrated in cut-out filters matching the molecular weight to approximately 2 ml before size exclusion chromatography. The protein fractions were checked in SDS-PAGE before concentrating and flash freezing in liquid nitrogen. Proteins were stored at -80°C.

Size exclusion chromatography

Size exclusion chromatography was conducted as a final polishing step in protein purification or in order to analyze protein-protein interactions.

Purified and concentrated proteins were subjected to size exclusion chromatography using either Superdex75 or Superdex200 16/60 columns (GE Healthcare) on an Äkta Prime Plus FPLC system (GE Healthcare) in order to visualize and exclude contaminated fractions.

Interactions of various recombinant proteins were analyzed using Superdex 75 or Superdex 200 10/300 or Superose 6 columns on an Äkta Purifier or Ettan LC system (both GE Healthcare).

Determination of protein concentrations

Protein amounts were determined by measuring the 280 nm absorption on a photometer (Eppendorf, Hamburg, Germany) using as a blank the same buffer the respective protein was dissolved in. From the absorption value, the protein concentration was calculated according to Beer's law ($A_{280nm} = \varepsilon \times d \times c$) by dividing it by the extinction coefficient ε (as predicted for the reduced state by the ProtParam tool) and multiplying it by the dilution factor.

Pull down experiments using GST-fused protein and GSH-sepharose beads

20 µl glutathione (GSH) sepharose beads were preequilibrated in buffer (25 mM HEPES 7.5, 150 mM NaCl, 1 mM DTT, centrifugation: 1.3 rcf, 4°C, 4 min) and mixed with the recombinant proteins of interest to a final concentration of 5 – 25 µM. The reactions were filled up with buffer to a final volume of 55 µl. After rolling for 1 h at 4°C, input samples (diluted 1:6) were taken and the beads were washed 3x in 4-10x volume of buffer. The beads were resuspended in 5 µl buffer and SDS samples were taken (diluted 1:10).

Quantification of protein interactions in pull down experiments

The interaction of two binding partners, one of which fused to GST was quantified from the Western Blots of pull down experiments. Scanned blots were analyzed using the Image software. Pictures were transformed into 8-bit format and black and white were inverted. The white intensity of the protein bands of interest was measured in an area comprising the whole band as narrow as possible. Background intensity was measured as well and subtracted from the values of the respective bands. In order to estimate the binding strength the intensities of the input GST-protein were related to the intensities of the pulled interaction partner. The wild type Atg19 was normalized to 100% binding of Atg8. On this basis the percentage of binding was calculated for the tested proteins.

Preparation of Giant Unilamellar Vesicles (GUV)

GUVs were prepared by electro formation at 35°C from lipid mixes containing 1 to 25 % DGS-NTA(1,2-dioleoyl-*sn*-glycero-3-[(N-(aminocarboxypentyl)iminodiaceticacid)succinyl] (nickel salt) and 85 % POPC (1-palmitoyl-2-oleoyl-*sn*-glycero-3-phosphocholine, both Avanti, AL, USA) depending on the experiment. They were labeled with rhodamine lipid dye at a concentration of 0.1 mg/ml (Avanti).

Coating of latex beads with protein

2 µm diameter latex beads (Invitrogen) were coated with protein by diluting the beads 1:1 in MES buffer (50mMMES, pH6, Sigma). Cross-linking was achieved by 2 h incubation of 50 µl 100 µM protein with 50 µl beads dilution and 400 µg EDAC (1,3-Propanediamine, N'-(ethylcarbonimidoyl)-N,N-dimethyl-, monohydrochloride). Afterwards the beads were washed 3x in buffer by spinning down at 10000 rpm at 4° for 10 min, removing the supernatant and resuspending in buffer. Protein coated beads were stored at 4°C.

Microscopy

Microscopy experiments were performed on a Spinning Disc microscope (Visitron Systems, Puchheim, Germany) using a 63x objective (Zeiss, Oberkochen, Germany). Pictures were acquired with the VisiVIEW Imaging software (Visitron Systems).

In order to assess the membrane binding capacities Atg19 in wild type and mutant versions was mixed with GFP-prApe1-coated latex beads of a diameter of 2 µm and incubated for 20 min at 4°C before spinning down at 2 rpm for 2 min. The supernatant containing unbound Atg19 was removed and the settled beads were resuspended in the same volume of buffer. The reactions were pipeted into Greiner plates (BD Biosciences, CA, USA), where first the GUVs, then C-terminally His-tagged Atg8 and after 10 min incubation Atg19 bound to meGFP-prApe1 propeptide coated beads were added.

Quantification of membrane bending in GUV experiments

The GUV-membrane bending capacities of different Atg19 mutants when binding to GFP-prApe1-propeptide coated latex beads were assessed by the visibility of a part of the rhodamine labeled membrane surrounding a green fluorescing latex bead. These events were counted. For each experiment two controls were tested; addition of Atg19 wild type and omission of the receptor.

III Results

In order to obtain further insights into the interaction between Atg8 and the autophagy-receptors Atg34 and Atg19 in presence and absence the of cargo, mutant versions of Atg8, Atg19 and prApe1 were generated (see Table 2). These were tested for their interaction qualities in different experimental set-ups.

Recombinantprotein	**Experiment(s)**	**Recombinant plasmid working name: "SMCx"**	**Plasmid vector**
Atg19 wild type	GST-pull down assay, SEC, GUV assay	159	pGEX-4-T-1
Atg19 W412A	GST-pull down assay, SEC, GUV assay	188	pGEX-4-T-1
Atg19 F376A	GST-pull down assay	438	pGEX-4-T-1
Atg19 F379A	GST-pull down assay	439	pGEX-4-T-1
Atg19 F376A, F379A	GST-pull down assay, GUV assay	440	pGEX-4-T-1
Atg19 F376A, W412A	GST-pull down assay	444	pGEX-4-T-1
Atg19 F379A, W412A	GST-pull down assay	445	pGEX-4-T-1
Atg19 F376A, F379A, W412A	GST-pull down assay, GUV assay	446	pGEX-4-T-1
Atg19 F376A, F379A, P385A, E386A	GST-pull down assay, SEC	450	pGEX-4-T-1
Atg19 F376A, F379A, P385A, E386A, W412A	GST-pull down assay, GUV assay	451	pGEX-4-T-1
Atg19 aa(365-415) F376A	GST-pull down assay	441	pGEX-4-T-1
Atg19 aa(365-415) F379A	GST-pull down assay	442	pGEX-4-T-1
Atg19 aa(365-415)F376A, F379A	GST-pull down assay, SEC	443	pGEX-4-T-1
Atg19 aa(365-415) F376A, W412A	GST-pull down assay	447	pGEX-4-T-1
Atg19 aa(365-415) F379A, W412A	GST-pull down assay	448	pGEX-4-T-1
Atg19 aa(365-415) F376A, F379A, W412A	GST-pull down assay, SEC	449	pGEX-4-T-1
Atg19 aa(365-415) F376A, F379A, P385A, E386A	GST-pull down assay, SEC?	452	pGEX-4-T-1
Atg19 aa(365-415) F376A, F379A, P385A, E386A, W412A	GST-pull down assay, SEC	453	pGEX-4-T-1
Atg19 aa(365-415)	GST-pull down assay, SEC	295	pGEX-4-T-1
Atg19 aa(365-407)	GST-pull down assay, SEC	309	pGEX-4-T-1
Atg19 aa(1-374)	GST-pull down assay	346	pGEX-4-T-1

Atg19 aa(1-384)	GST-pull down assay	347	pGEX-4-T-1
Atg19 aa(1-396)	GST-pull down assay	348	pGEX-4-T-1
Atg19 aa(376-415)W412A	GST-pull down assay	349	pGEX-4-T-1
Atg19 aa(386-415)W412A	GST-pull down assay	350	pGEX-4-T-1
Atg19 aa(398-415)W412A	GST-pull down assay	351	pGEX-4-T-1
Atg19 aa(365-415) W412A	GST-pull down assay, SEC	298	pGEX-4-T-1
Atg19 aa(1-123)	GST-pull down assay, SEC	306	pGEX-4-T-1
Atg19 (124-254)	GST-pull down assay, SEC	307	pGEX-4-T-1
GST-Atg8/Atg8(-6xHis)	GST-pull down assay/SEC, GUV assay	437/58	pGEX-4-T-1/pEtDuet
(GST-)prApe1 aa(1-45)/eGFP-prApe1	GST-pull down assay, SEC/GUV assay	308	pGEX-4-T-1/pmeGFP-C1

Table 2: Recombinant proteins generated for this thesis
The cDNA encoding the respective protein was cloned into the indicated plasmid vectors, via the pGEX-4T-1-vector an N-terminal GST-tag was fused to the protein, via the pEtDuet-vector an N- or C-terminal 6xHistidine tag was fused to the protein. These tags were proteolytically cleaved if required. The proteins were tested in the indicated experimental set-up(s).

Protein purification

In the following the purification of Atg8 from a 6xHis-TEV-Atg8 construct is described representing the general procedure and results of protein purification.

The cDNA encoding for the protein with an additional tobacco etch virus protease (TEV-) cleavage site at the 5' end was generated by PCR and cloned into the pETDuet plasmid vector (to add a 6xhistidine tag). This construct was transformed into an *E.coli* strain especially designed for protein expression (Rosetta pLysS, see Methods) and the protein was expressed under adequate conditions (temperature, medium, concentration of IPTG for induction of expression, see Methods). After cell lysis and clearance of insoluble contents from the lysate, the protein was affinity-purified according to the tag conferred from the vector (glutathione-S-transferase (GST) or 6xHis). 6xHis-Atg8 was purified by binding it to a Ni-column and subsequently eluting it with a step wise gradient of imidazole (10-300 mM, see His trap profile Figure 5 (A) and (B)). The fractions of where the recorded UV absorption (280 nm) reached a local maximum in 50-150 mM imidazole were loaded on a coomassie gel to detect the protein of interest and visualize contamination or degradation, as seen by additional protein bands. Atg8 was detected in fractions 187-191 ml (100 mM imidazole) and 210-212 ml (150 mM imidazole, see Figure 5).

A

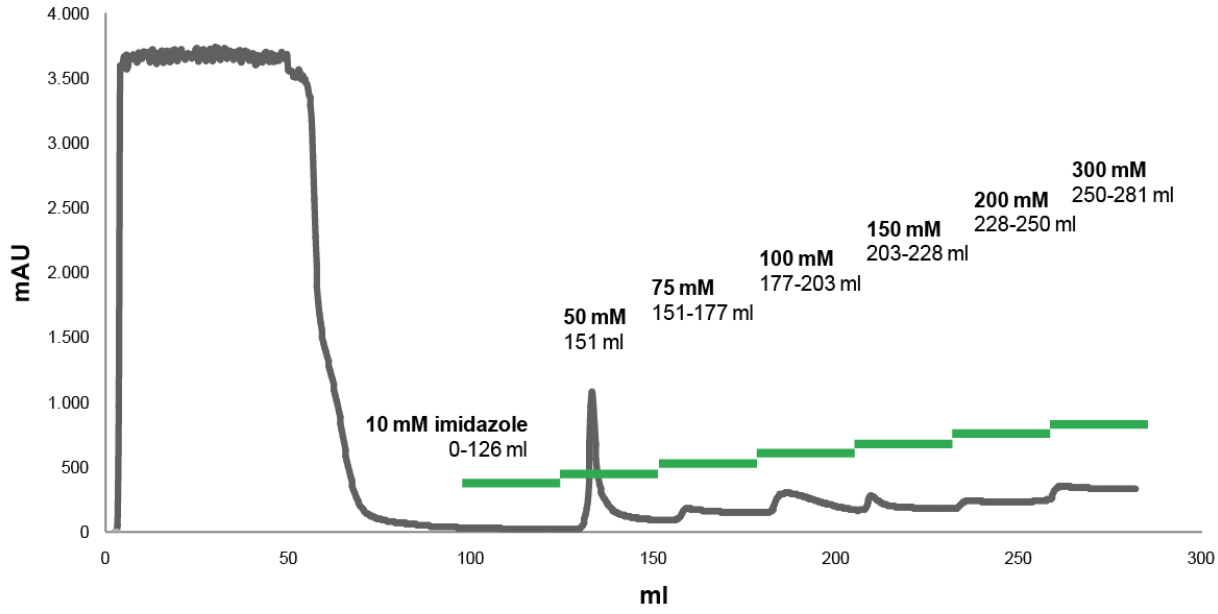
4.000
3.500
3.000
2.500
2.000
1.500
1.000
500
0
mAU
0
50
100
150
200
250
300
ml
10 mM imidazole
0-126 ml
50 mM
151 ml
75 mM
151-177 ml
100 mM
177-203 ml
150 mM
203-228 ml
200 mM
228-250 ml
300 mM
250-281 ml

B

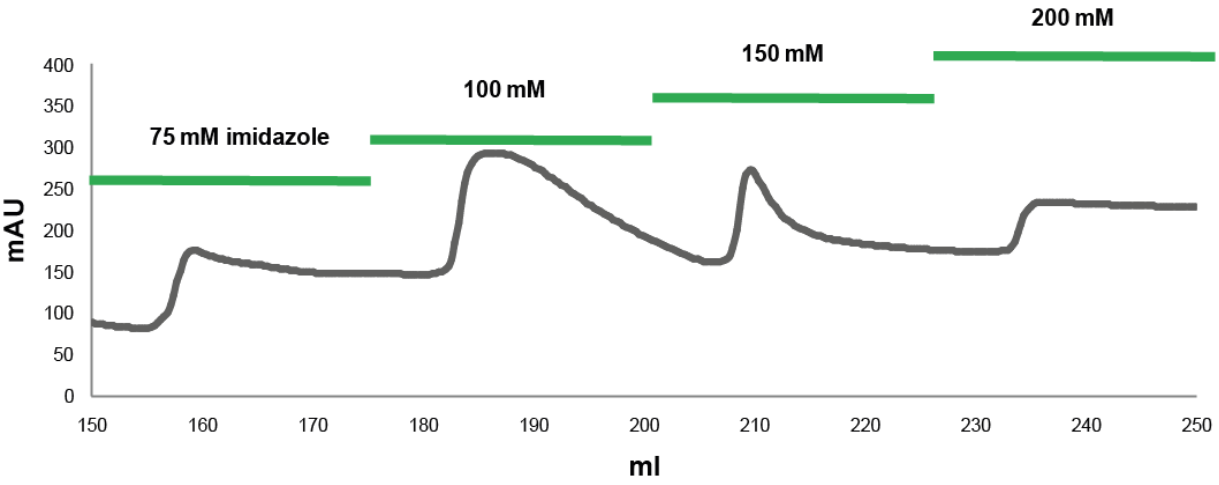
400
350
300
250
200
150
100
50
0
mAU
150
160
170
180
190
200
210
220
230
240
250
ml
75 mM imidazole
100 mM
150 mM
200 mM

C

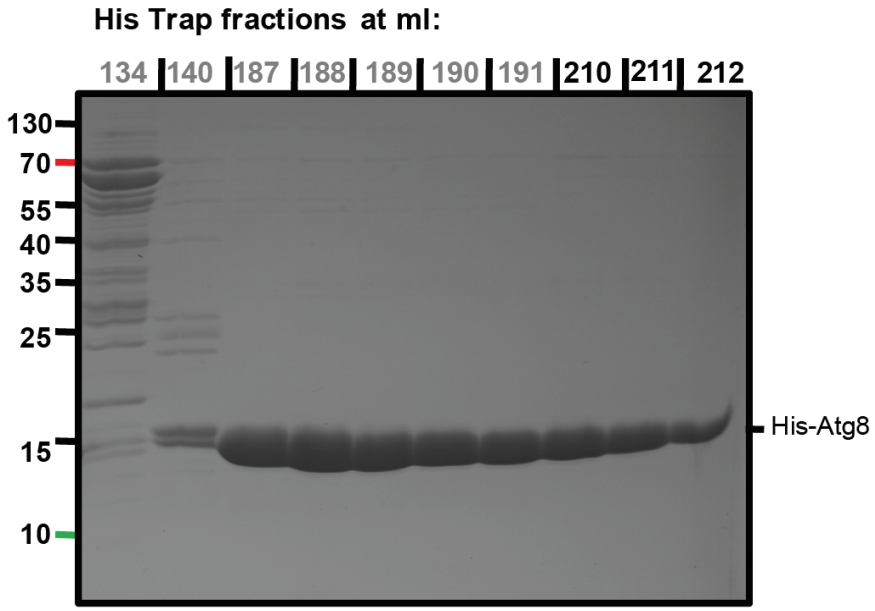

Figure 5: HisTrap purification of 6xHis Atg8
(A) UV profile of the complete HisTrap. (B) Enlarged profile of the fractions at 75-200 mM imidazole. Green lines indicate step-wise increase of imidazole concentrations (see labels). (C) Several HisTrap fractions were loaded on a CBB gel. 6xHis-Atg8 was detected in imidazole concentrations of 100 and 150 mM imidazole. The fractions of 134 and 140 ml correspond to imidazole concentrations of 50 mM and 75 mM imidazole respectively. Fractions 187-191 ml correspond to 100 mM imidazole (gray labels) and fractions 210-212 ml to 150 mM (black labels). These latter were pooled separately and subjected to FPLC (shown in the following for the 210-212 ml fractions). Scaling on the left indicates molecular weight in kD.

The fractions of each salt concentration containing the protein were pooled separately. The fact that the protein eluted in different imidazole concentrations might imply that these two pools differ in their folding or oligomerization state. Since in lower salt concentrations non specific ionic interactions are favored as compared to an increased salt concentration, it might be the case that the 100 mM imidazole fractions contain more misshaped Atg8 molecules and therefore they could not bind the Ni-resin of the column properly. The pooled protein fractions were concentrated to approximately 2 ml by centrifugation in filtering tubes. Purified TEV-protease was added to cleave off the 6xHis tag. Cleavage efficiency was monitored on a Coomassie gel (not shown, compare shift of His-Atg8 to Atg8-bands in Figure 7). As a final polishing step, the cleaved Atg8 was subjected to size exclusion chromatography (Figure 5 (A)). The peak fractions (67-74 ml) were loaded on a coomassie gel (Figure 5 (B)). The fractions of 69-71 ml were pooled as a large amount of protein but no contaminants were detected (Figure 5 (B)).

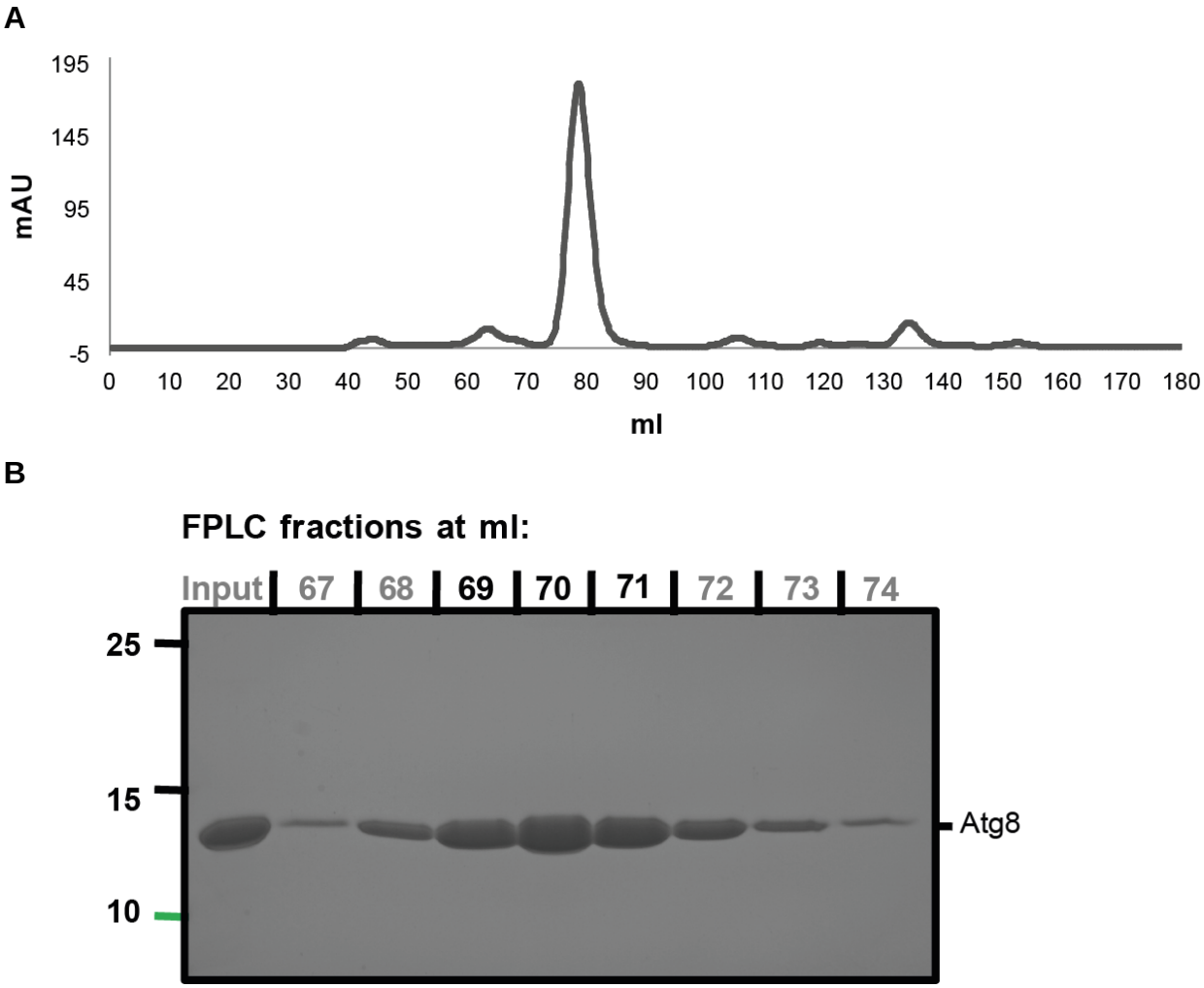

Figure 6: Size exclusion purification of Atg8
(A) UV profile of Atg8 in FPLC. (B) The input and the peak fractions of the FPLC were loaded on a CBB gel (as indicated). Scaling on the left indicates molecular weight in kD.

The concentration was estimated by determining the absorption of UV light (280 nm) of the protein solution. According to the Lambert-Beer law, the absorption of a solution equals the product of the extinction coefficient of the component (here protein), the width of the layer (1 cm) and the concentration of the component. Thus, the protein content of the gained solution could be calculated. This theoretical concentration was confirmed by loading corresponding amounts of protein (1.5 and 3 µg) on a CBB gel (Figure 6). Proteins were flash frozen and stored at -80°C. In Figure 7 the crude lysate of cells expressing His-Atg8 as well as the soluble fraction thereof and the purified Atg8 can be compared.

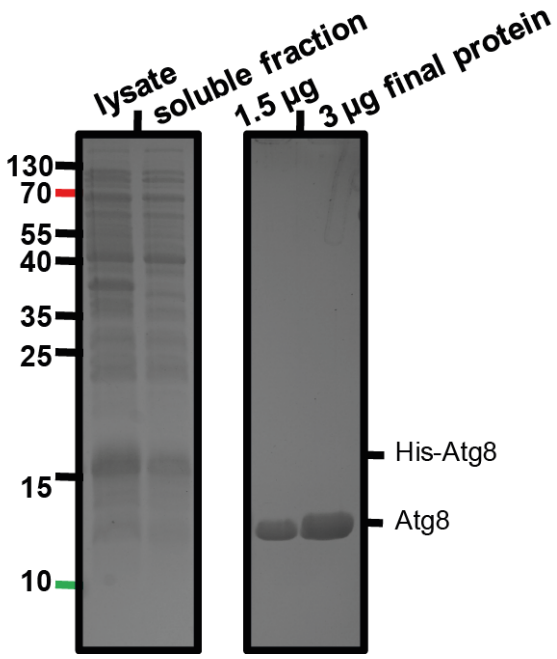

Figure 7: Bacterial lysate and purified protein of Atg8 expression.
Overexpressed 6xHis-Atg8 is detected in SDS-PAGE in the crude cell lysate and in the soluble fraction thereof (lanes 1 and 2 on the left). 1.5 and 3 µg of purified Atg8 were loaded to verify the correct concentration (lanes 3 and 4 on the right). Scaling on the left indicates molecular weight in kD. Note the band shift of 6xHis-Atg8 at around 15 kD to Atg8 at around 13 kD. This is due to cleavage of the His-tag by TEV-protease.

Pull-down experiments using GST-tagged protein and glutathione-sepharose beads

In order to identify Atg8 binding sites in the receptor molecule Atg19, the recombinant proteins of interest were tested for interaction in pull down experiments. Several proteins were mutated at suspected Atg8 interaction sites or these sites were completely removed, as described in detail in the following. After incubation, GST-fused proteins as well as respective binding partners could be detected in the fraction of the washed beads via Coomassie staining or western blotting.

A GST fused version of the wild-type Atg19 was shown to bind Atg8 (indirectly) to the beads (Figure 9 (A) and (C)). Comparing this amount of Atg8 as observed by western blotting to the respective amounts in experiments using N-terminally or C-terminally truncated GST-Atg19, points to a reduced binding strength the shorter the Atg19 constructs (Figure 9 (C)).

To narrow down the amino acid sequence in Atg19 responsible for this binding, three versions of Atg19 truncated from the C-terminus (Atg19 aa1-374, Atg19 aa1-384, Atg19 aa1-396) and three versions of the C-terminus truncated from the N-terminus (Atg19 aa376-415, Atg19 aa386-415, Atg19 aa398-415) containing the W412A mutation were cloned and purified (Figure 8). Western blotting and subsequent quantification of the white values of the Atg8 bands using ImageJ software shows that Atg8 binding is reduced in the truncation mutants as

compared to wt Atg19 (Figure 9 (A) and (C) and Figure 10 (A)) or wt Atg19 C-terminus (Figure 9 (B) and (C) and 10 (B)), which were normalized to 100% binding (Figure 10). Equal amounts of protein in the reactions were checked by loading the input fractions on a CBB gel (Figure 9 (A) and (B)). Interestingly Atg19 C-terminus bound stronger to Atg19 wt full length in wt as well as in a LIR mutant (W412A) version (compare in Figure 9 (C) bands 1 with 7 and 8). The interaction of the C-termini with Atg8 was already detectable on the CBB gel as opposed to Atg19 full length, where no bound Atg8 was detected by CBB (compare band 2 in Figure (A) with bands 2 and 4 in (B)). This hints to a stronger binding of the C-terminal domain to Atg8.

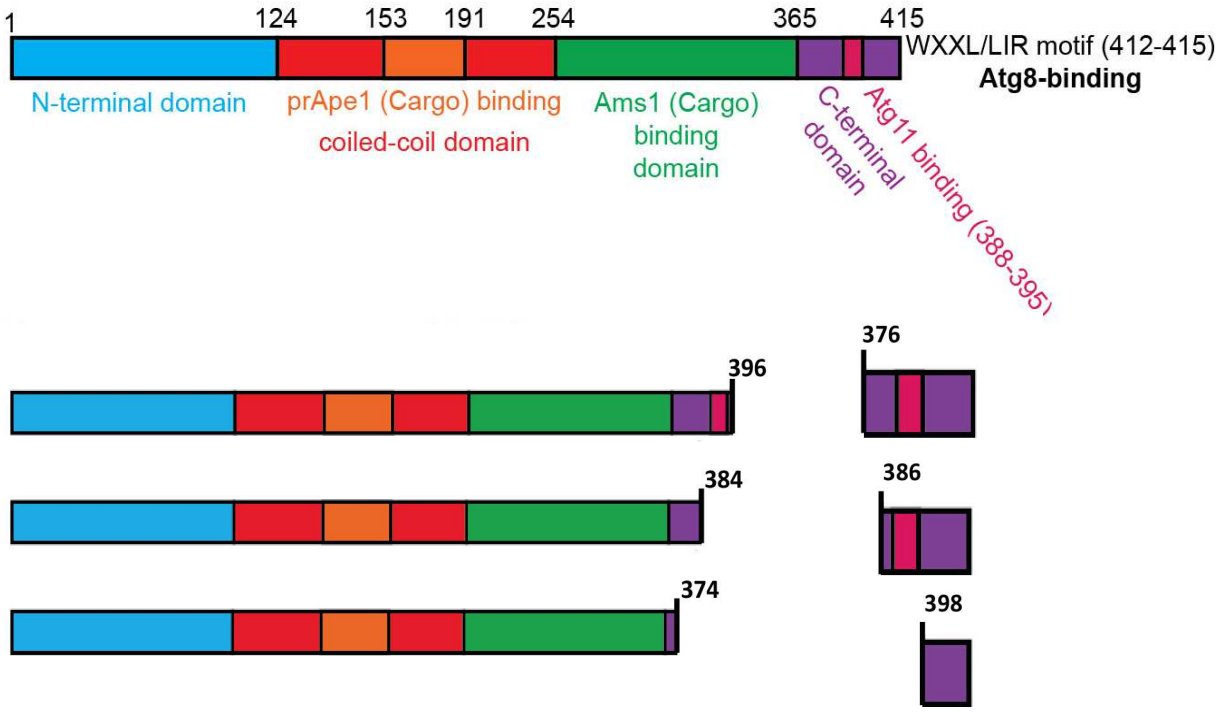

Figure 8: Truncation mutants of Atg19 tested for Atg8 binding.
Top: Domain organization of Atg19, domains are shown in different colors, amino acid number on top. Bottom left: C-terminal truncations. Right: N-terminal truncations bearing the W412A mutation.

In Atg19 aa1-374 binding of Atg8 seems to be weakest (37%, Figure 9 (C) and 10 (A)), increasing in Atg19 aa1-384 (53%) and more so in Atg19 aa1-396 (56%). On the other hand, Atg19 aa376-415 W412A showed a stronger Atg8-interaction than Atg19 aa386-415 W412A (55% vs. 25%, Figure 9 (C) and 10 (B)). In the shortest C-terminal construct, Atg19 398-415 W412A, binding seems to be reduced as well (25%, Figure 9 (C) and 10 (B)). As a reference Atg19 aa365-415 in wt and W412A (LIR mutant used to exclude background Atg8 binding via the LIR motif), were loaded. The C-terminal constructs seemed to bind a higher amount of Atg8 than full length Atg19 (compare Atg8 bands in Figure 9 (A) vs. (B) or in (C)). These

experiments were also conducted with a GST-tagged version of Atg8 and untagged Atg19 constructs with C-terminal truncations confirming the upper results (Figure 9 (D)). The Atg19 mutants truncated from the N-terminus could not be detected using CBB staining because of their very low molecular weight.

A

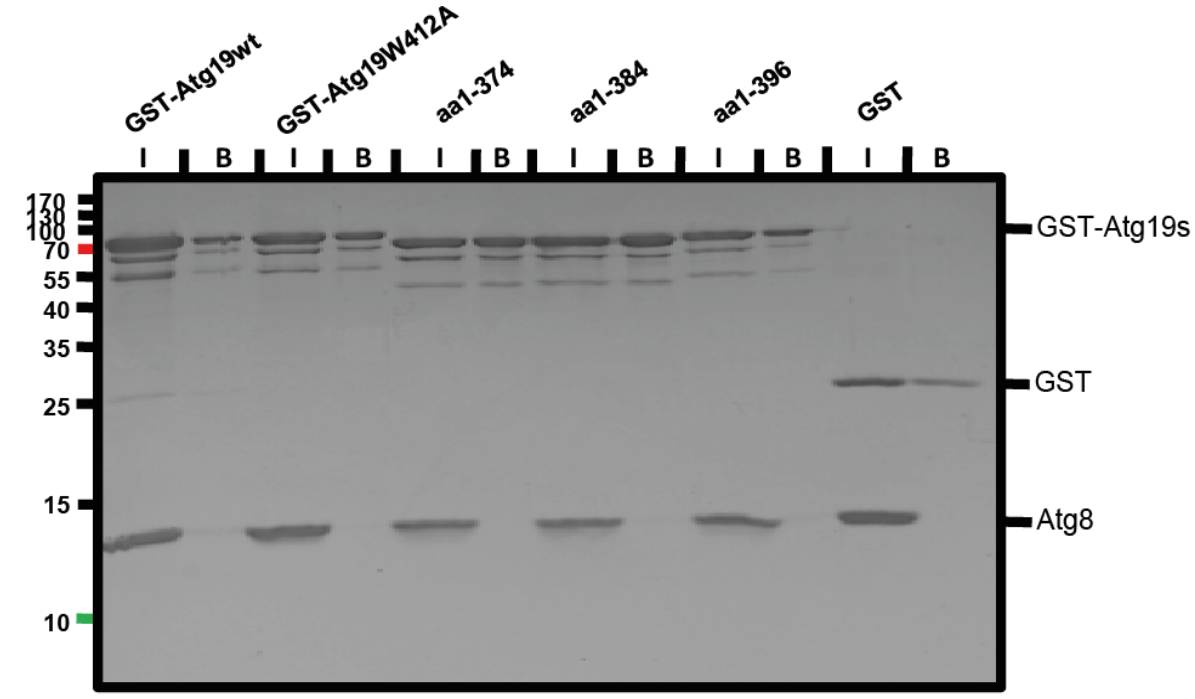

B

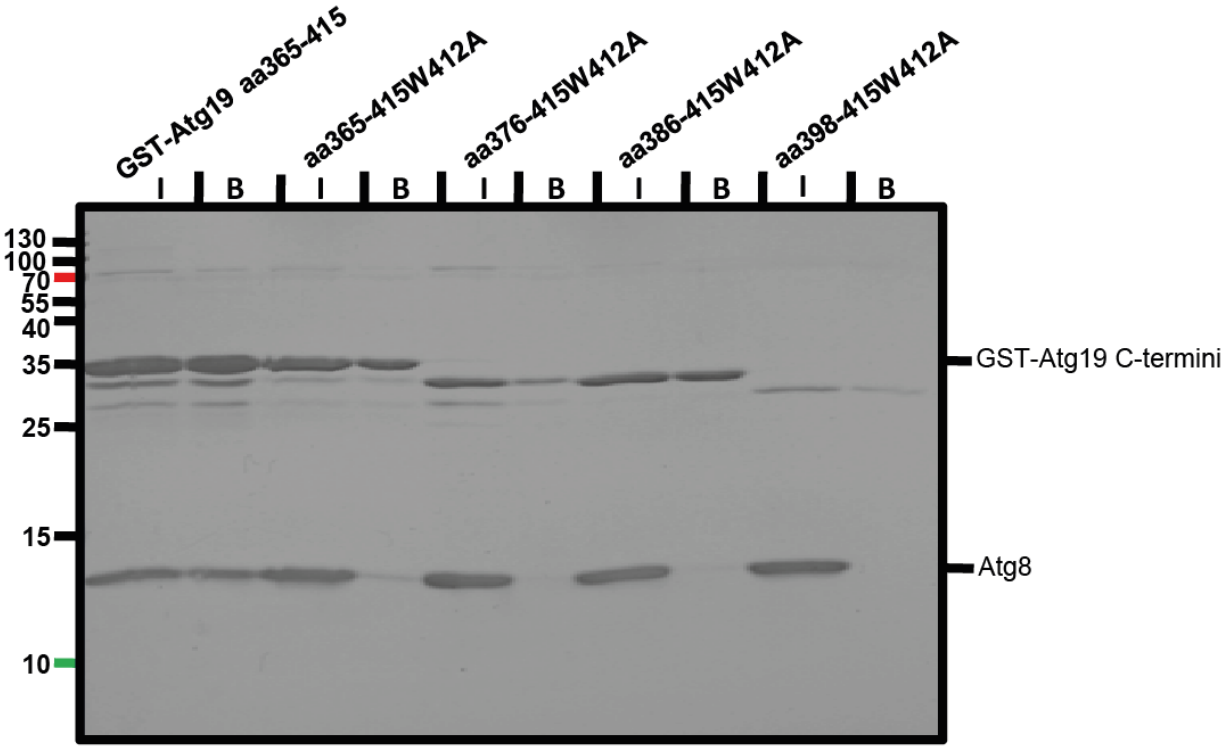

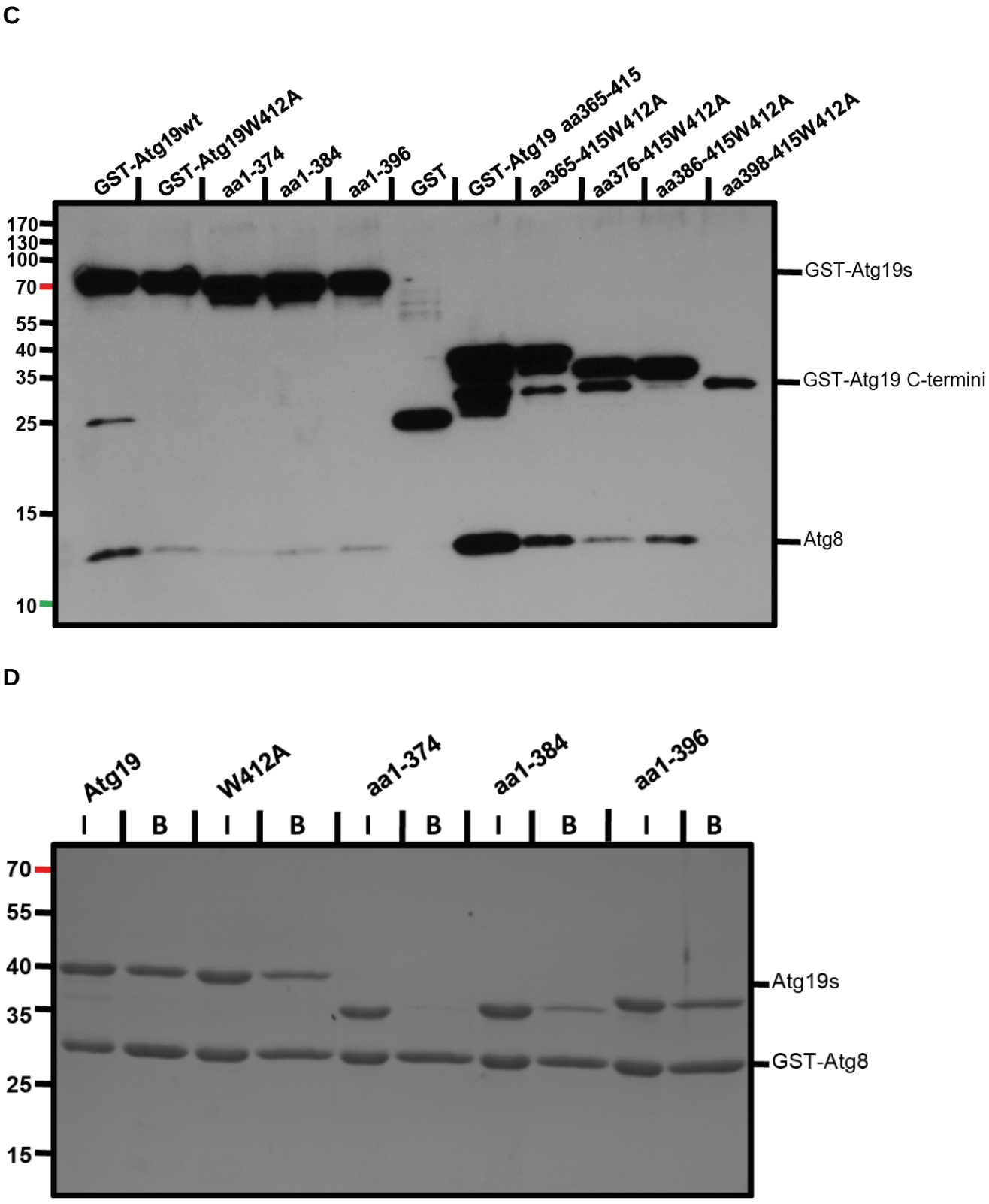

Figure 9: Pull downs of GST-fused Atg19 truncation mutants and untagged Atg8.
Coomassie Brilliant Blue stained input (I) and interaction partners pulled down along with the beads (B) of Atg8 and C-terminally (A) or N-terminally (B) truncated GST-Atg19 mutants (as indicated). (C) Anti-GST-Atg8 (rabbit) Western Blot of pulled down fractions, loading as indicated. (D) CBB stained input (I) and pulled down fractions (B) of GST-Atg8and N-terminally truncated Atg19 mutants (as indicated). Scaling on the left indicates molecular weight in kD.

A

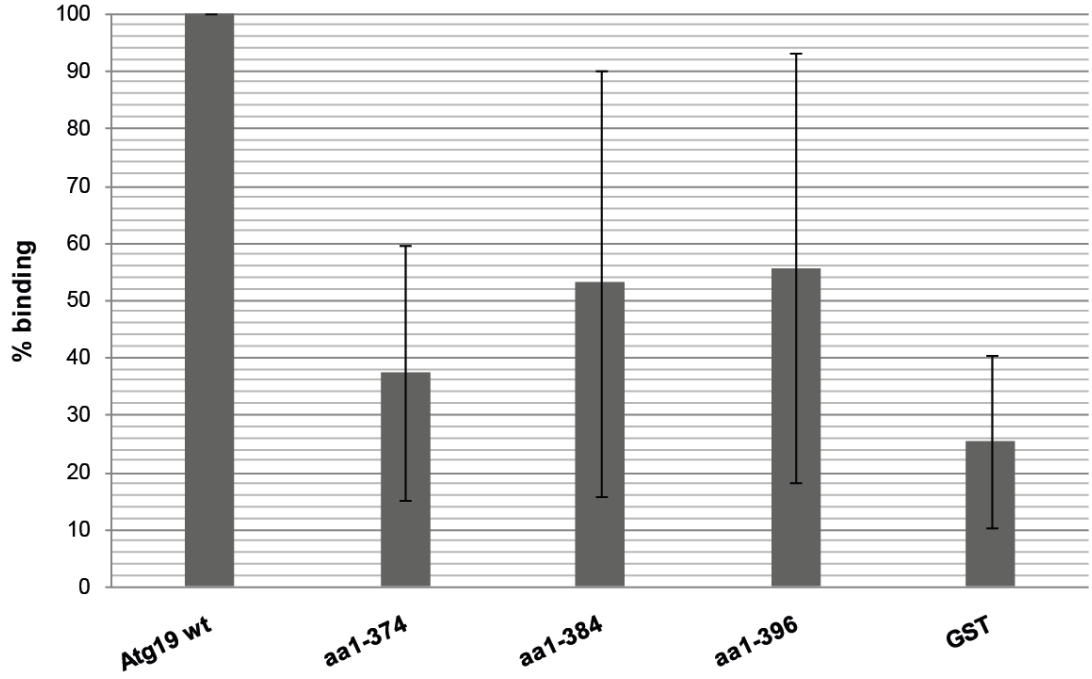

B

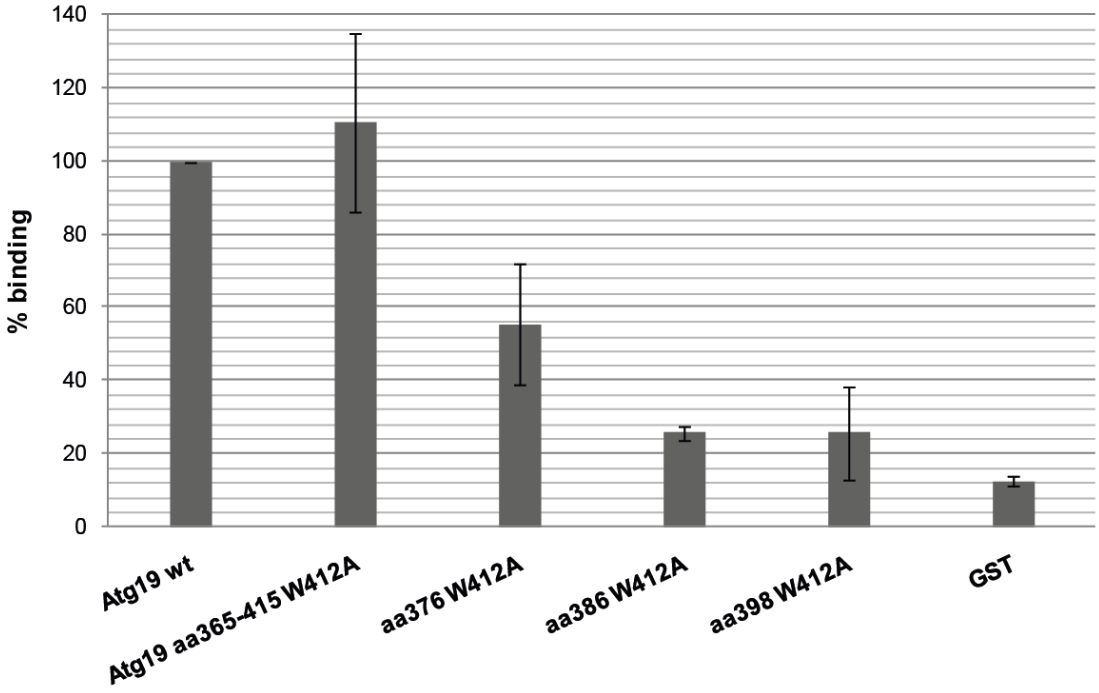

Figure 10: Quantification of Atg8 binding of Atg19 truncation mutants
Western Blots of the respective pull down experiments were analyzed using the ImageJ software. White intensities of the Atg8 bands in the beads fractions were measured, from these values the strength of Atg19-Atg8 interaction was inferred, the intensity of Atg8 bound to Atg19 wt full length (A) or C-terminus(B) was normalized to 100% binding. y-axis: Percentage of Atg8 binding of the respective mutant as compared to wt Atg19 full length (A) or C-terminus (B). x-axis: Atg19 mutants. Bars: Standard deviation. Quantifications are based on three independent experiments.

From these experiments it becomes evident that there are several Atg8 binding sites in Atg19's C-terminal domain. One of these residing before aa374 because Atg8 binding is observed in this shortest of the C-terminal truncation mutants (Atg19 aa1-374, Figure 9 (C) and (D)). Since the amount of bound Atg8 increases with the length of the Atg19 mutants, more binding sites could be between aa374 and 384 and aa384 and 396 respectively. The decrease in Atg8 binding was going along with shortening of the molecule from the N-terminus aa376/386/398-415 corroborates this finding.

Furthermore it was found that the C-terminal domain of Atg19 binds stronger to Atg8 than the full length molecule (compare beads fractions of wt full length Atg19 in **Figure 9**Figure 9 (A) and (C) and wt C-terminus of Atg19 in Figure 9 (B) and (C) and quantification of wt full length Atg19 and C-terminus W412A mutant in Figure 10 (B)). This confirms previous results (JSM).

Atg19's C-terminal domain contains a four amino acid stretch (FYSF) resembling a LIR-motif (WxxL, see Figure 11). This motif is not present in Atg34, which has been shown to be defective in Atg8 binding when its C-terminal LIR motif is silenced (W409A)[51]. But it aligns to a LIR motif in the mammalian autophagy receptor p62, suggesting its role for binding Atg8.

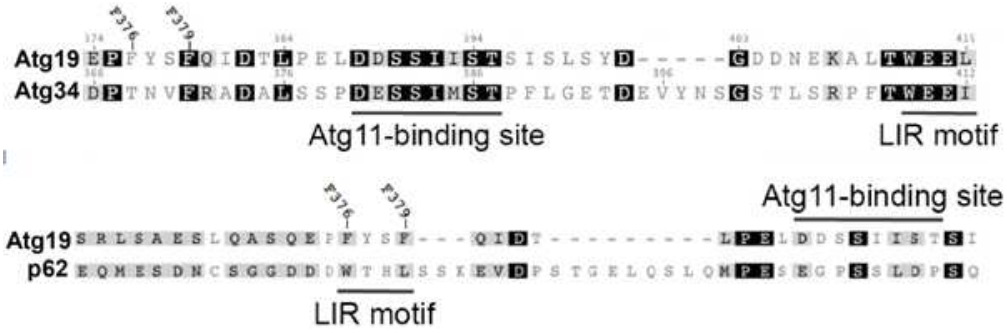

Figure 11: Alignment of the amino acid sequences of the yeast autophagy receptors Atg19 and Atg34 and Atg19 and mammalian p62 respectively
An FYSF sequence at aa376-379 is not present in Atg34, but aligns to a W-LIR motif in the mammalian autophagy receptor p62. A PE motif at aa384-385 of Atg19 is present in p62. But not in Atg34. These sites were tested for their involvement in binding to Atg8. The Atg11 binding site (not present in p62) as well as the LIR motifs are indicated.

In order to test if the two phenylalanines (F376 and F379) are involved in Atg8-binding they were mutated to alanines in a wt and LIR mutant (W412A) background either individual or in combination. These mutants were used for GST-pull down experiments as described above. In a qualitative pull down experiment, the Atg19 F376A mutant pulled less Atg8 than the wild type, in full length as well as in a C-terminal domain-only construct. Binding was also, but to a less extent decreased when F379 was mutated to alanine (Figure 12). When both

phenylalanines were exchanged interaction with Atg8 was even more decreased. In a W412A background these results could be corroborated showing a lower overall binding of Atg8 (Figure 12). The same effect was observed in the C-terminal domain of Atg19 and mutant versions thereof (Figure 13).

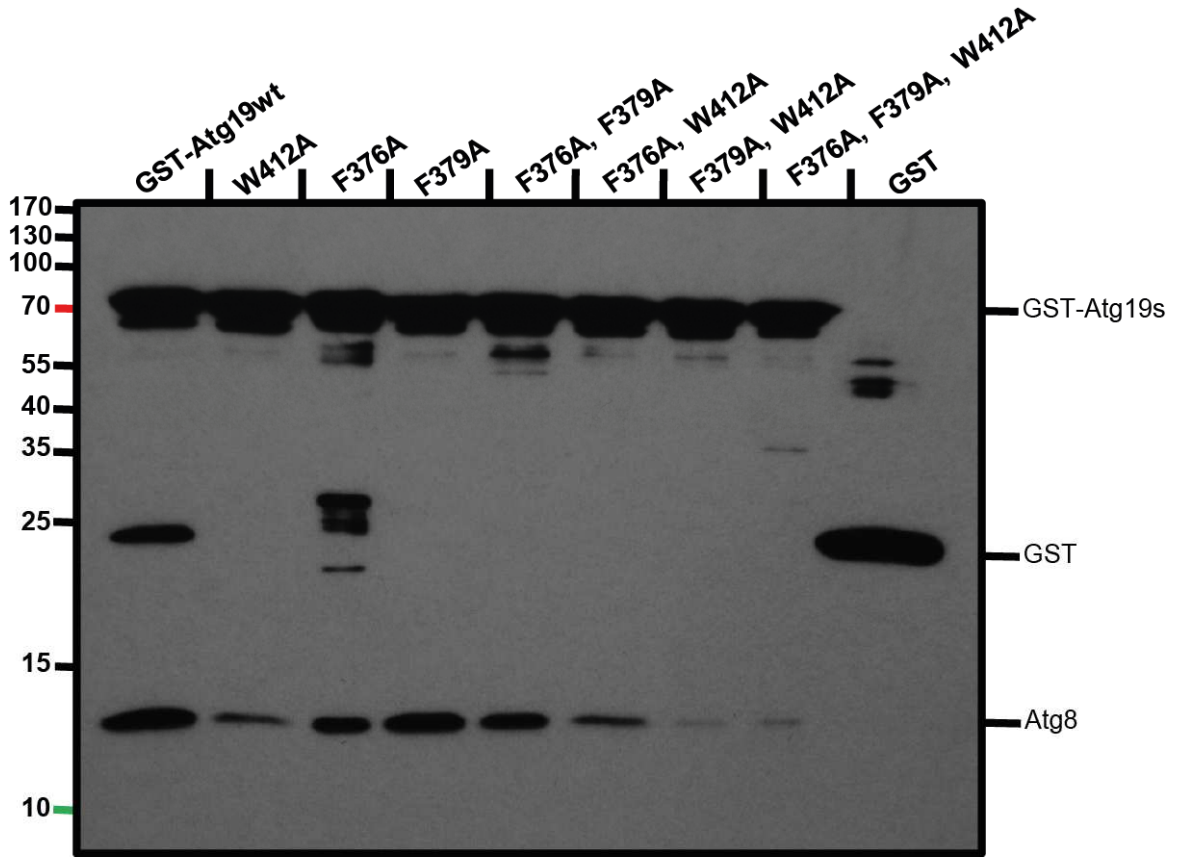

Figure 12: Pull downs of GST-fused Atg19 F and W mutants and untagged Atg8.
Anti-GST-Atg8 (rabbit) Western Blot of pulled down fractions, loading as indicated. Scaling on the left indicates molecular weight in kD.

These experiments were also conducted with a GST-tagged version of Atg8 and Atg19 constructs without GST confirming the results (not shown). Taken together, these results suggest that the FYSF-sequence in Atg19's C-terminal domain is another binding site for Atg8.

Nevertheless, low amounts of Atg8 (above background levels, compare to GST-control in Figure 12 and 13) could be detected in the full length and the C-terminal F376A, F379A, W412A mutants by western blotting (Figure 12 and 13) hinting on yet another Atg8 interaction site in the C-terminus of Atg19.

Another potential Atg8 binding site could be a PE sequence in the C-terminus of Atg19. This motif (aa385-386) is localized immediately N-terminal to the known Atg11 binding site (aa388-395)[59]. Furthermore this PE motif is also present in the mammalian autophagy receptor p62 (which has no Atg11 binding site, since there is no homologue thereof in higher

eukaryotes) suggesting its involvement in receptor function, in this case binding of Atg8 like molecules. It is not conserved in the Atg34 receptor, which is assumed not to have any other Atg8-interaction site apart from its C-terminal LIR motif (see Figure 11). P385 and E386 were therefore tested for their role in Atg8 binding. Both amino acids were mutated to As simultaneously in Atg19 C-terminus with a W412A and a F376A, F379A, W412A mutation background in order to test their effect on Atg8 binding excluding background binding by the other two binding sites. To estimate the binding capacities of these mutants, Atg19 C-terminus in wt, W412A mutant, F376A, F379A mutant or F376A, F379A, W412A mutant were tested in comparison. When the PE sequence was mutated in a F376A, F379A background Atg8 binding decreased to 18% as compared to the wild type (Figure 13). When W412A is mutated additionally the binding goes down to a background level of 6% (7% in the GST only control).

A

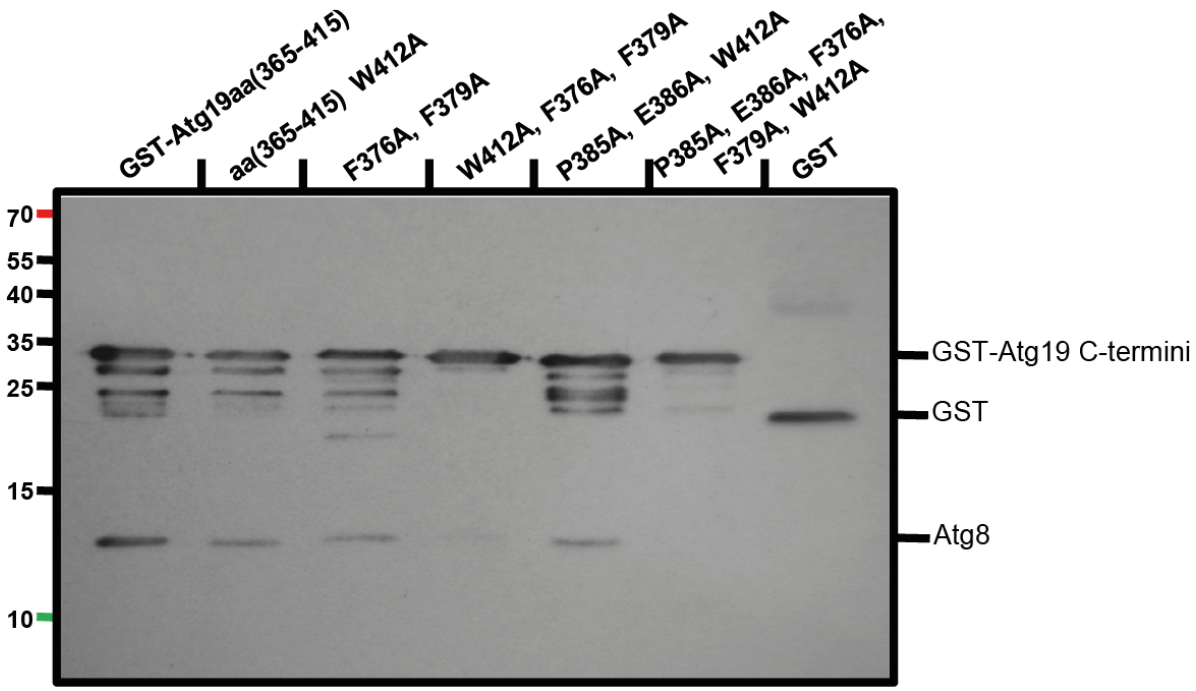

B

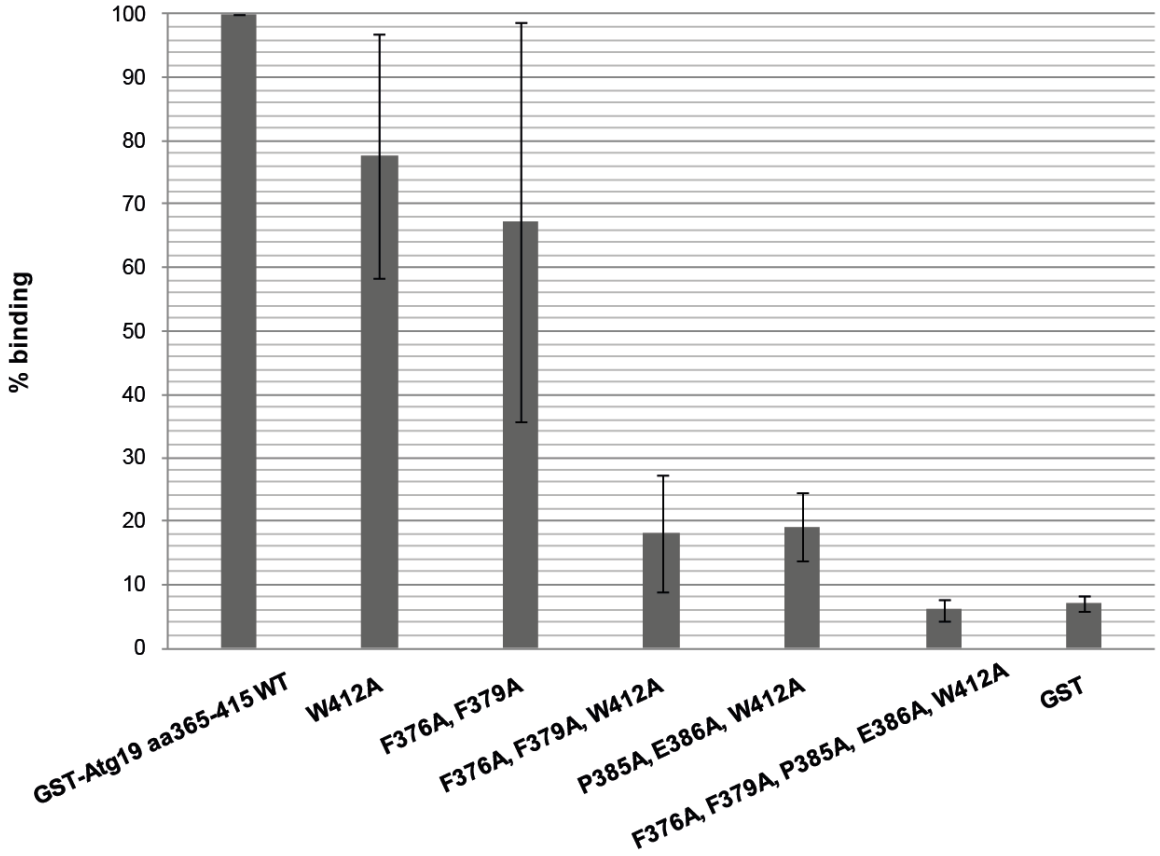

Figure 13: Pull downs of GST-fused Atg19 C-terminus F, W and P+E mutants and untagged Atg8.
(A) Anti-GST-Atg8 (rabbit) Western Blot of pulled down fractions, loading as indicated. Scaling on the left indicates molecular weight in kD. (B) Quantification of Atg8 binding. Bars: Standard deviation. Quantifications are based on three independent experiments.

For further confirmation of the upper results, GST-pull downs were conducted using GST-fused prApe1-propeptide (aminoacids1-45) to indirectly show the binding of Atg19 and Atg8. Since Atg19 interacts with prApe1-propeptide[59] as well as Atg8[60], Atg19 would be expected to bind to propeptide and Atg8, mediating an indirect interaction of Atg8 and the GST-propeptide-covered beads. In this set-up the GST- fused propeptide is locally concentrated on the GSH-beads since GST interacts strongly with GSH. This also implies that the propeptide faces the surface of the beads. This mimics the in vivo situation where the propeptide protrudes from prApe1 oligomeres and mediates interaction with other prApe1 oligomeres as well as the autophagy machinery via binding of the receptor Atg19[67]. Purified GST-propeptide was mixed with Atg19 wild type and different mutant versions and Atg8.

Western blotting using the GST-Atg8 antibody showed a decreasing recruitment of Atg8 to the propeptide-covered beads by the F376A, F379A, the W412A, the F376A, F379A,

W412A, the P385, E386, W412A and the F376A, F379A, P385, E386, W412A mutants (Figure 14).

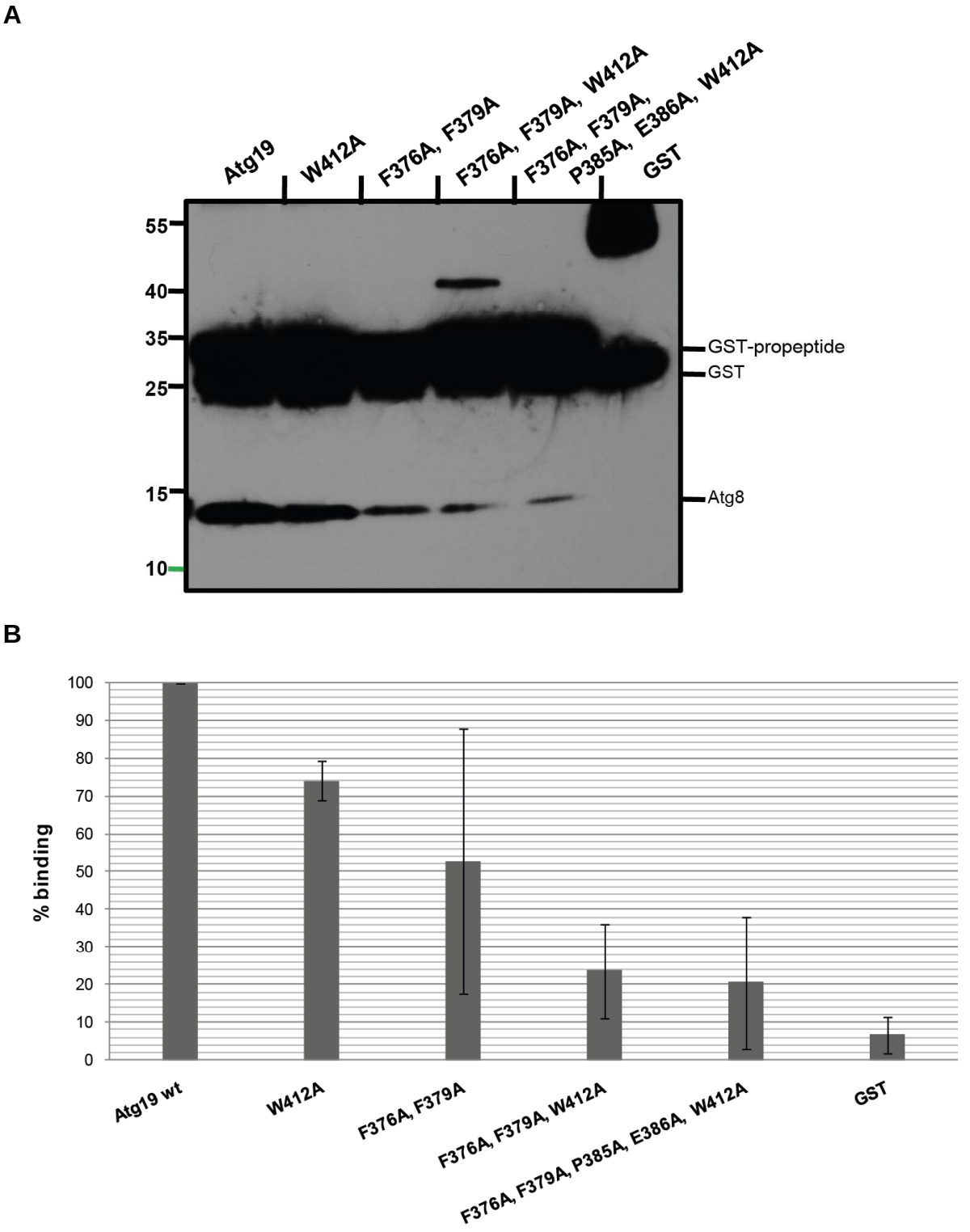

Figure 14: Pull downs of GST-fused prApe1 propeptide and Atg19 F, W and P+E mutants and untagged Atg8.
(A) Anti-GST-Atg8 (rabbit) Western Blot of pulled down fractions, loading as indicated. (B) Quantification of Atg8 binding. For quantification shorter exposed films were used. Bars: Standard deviation. Quantifications are based on three independent experiments.

Analytical size exclusion chromatography to estimate the saturation point of Atg19 C-terminus and Atg8 binding

High pressure liquid chromatography was performed to study the interaction of Atg19 C-terminal domain (aa365-415) in wild type or LIR-mutant (W412A) and Atg8. The saturation point of Atg19 C-terminus and Atg8 complexation, i.e. the Atg8 concentration at which no further binding to Atg19 C-terminus occurs, can be inferred from the stability of the UV-absorption peak of this complex. These experiments were conducted in order to confirm that Atg19 C-terminal domains binds more Atg8 molecules than the W412A mutant, but also to test if this latter protein is still able to form a complex with Atg8. Furthermore, the saturation point of the interaction, i.e. the molar ratio of Atg19 C-terminus to Atg8 at which no further Atg8 molecules will be bound by Atg19 C-terminus can be estimated. The Atg19 C-terminal domain and Atg8 were mixed in different molar ratios, keeping the concentration of the Atg19 C-termini constant at 40 µM (230 ng/ml) and increasing the concentration of Atg8 from 40 µM (550 ng/ml) to 120 µM in steps of 20 µM. The reactions were incubated at 4°C for 30 minutes. The UV-absorption of the reaction mixes were recorded and analyzed using the UNICORN software.

The Atg19 C-terminal domains eluted at 1.30 ml, Atg8 at 1.39 ml and the complex of these two eluted at 1.22 ml (wt) or 1.25 ml (LIR-mutant) (Figure 15).When all Atg8 molecules are bound to the Atg19 C-terminal domain, only the UV-absorption peak of the complex at 1.22 ml (wt) or 1.25 ml (LIR-mutant) was observed (Figure 15 and Table 3). Increasing Atg8 the amount of Atg8 in the reaction resulted in the appearance of a second peak at a retention volume of 1.39 ml representing uncomplexed Atg8. From the ratio of Atg19 C-terminus to Atg8 in the saturated complexation reactions, the binding capacity of Atg19 C-terminal domain in wt or LIR-mutant version could be estimated. Several UV absorption profiles are shown in Figure 15 (A) and (C) for wt Atg19 C-terminal domain and W412A mutant respectively. The UV absorption curve of Atg19 C-terminal domain are depicted to visualize the shift of their peak absorption towards a lower retention volume (i.e. higher molecular weight) when Atg8 is added. This represents the formation of a complex of these two proteins, which has a higher weight that the C-terminus alone. Figure 15 (A) and (C) respectively show two absorption curves of this complex, one at a molar ratio of 1 to 0.5 (Atg19 C-terminus:Atg8) and the other at a molar ratio of 1 to 2.5 (Atg19 C-terminus : Atg8). The former profile suggests that all added Atg8 is complexed, since only the absorption maximum of the complex at 1.22 ml (wt) or 1.25 ml (W412A) is observed, but no peak of unbound Atg8 detected (at 1.39 ml). This changes when Atg8 is added in an excess of 2.5

molcules over one molecule of Atg19 C-terminus. In this situation, a UV absorption peak appears at 1.39 ml, similar to the profile observed in a control run of Atg8 alone (compare Atg8 peak in control runs and in complexation runs at 1.39 ml in Figure 15 (A) and (C)). The saturation of the Atg19 C-terminus-Atg8 complex is also shown in Figure 15 (B) and (D). In low ratios of Atg19 C-terminus to Atg8 (1:1) only one UV-peak is observed, indicating that all added Atg8 is bound to Atg19 C-terminus. Note that in W412A (Figure 15 (D)) a smaller peak at the right side of the prominent complex peak is appearing in the curve, suggesting that more Atg8 is already unbound here as compared to wt Atg19 C-terminus. With increasing ratios (up to 1:4 Atg19 C-terminus:Atg8) higher amounts of unbound Atg8 can be observed in the UV curves. These are represented by a constant rise of the absorption maximum at 1.39 ml.

Recombinant protein	Retention volume HPLC [ml]	Concentration	Extinction coefficient
Atg19 aa365-415	1,30	40 µM	8480
Atg19 aa365-415 W412A	1,32	40 µM	2980
Atg8	1,39	40-400 µM	2980
Atg19 aa365-415-Atg8 complex	1,22		
Atg19 aa365-415 W412A-Atg8 complex	1,25		

Table 3: Retention volumes of Atg19 C-termini, Atg8 and the complex of these on an Ettan HPLC system.

The UV absorption peak of wild type Atg19 C-terminus stabilized at a ratio of 1:4 molecules of Atg19 C-terminus to Atg8 suggesting a saturation of the Atg19-Atg8 complex at an excess of 4 molecules Atg8 over one molecule of Atg19 C-terminus (Figure 15 (B)). In contrast, the peak of LIR-mutant Atg19 C-terminus stabilized at a ratio of 1: 2.5 Atg19 C-terminus to Atg8 molecules hinting to a binding capacity in the range of 2-3 molecules Atg8 by Atg19 C-terminal domain in W412A (Figure 15 (D)).

A

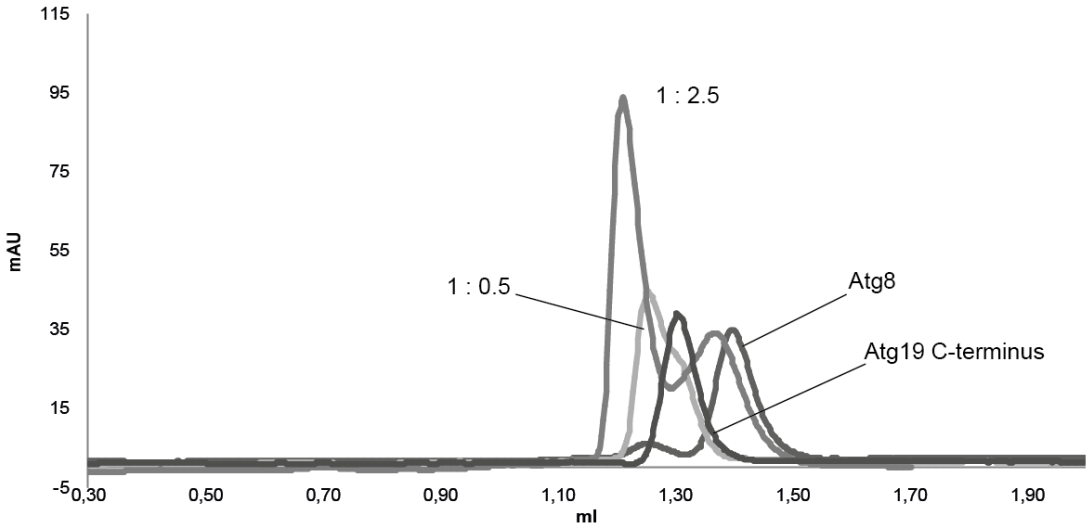
115
95
75
55
35
15
-5
mAU
0,30
0,50
0,70
0,90
1,10
1,30
1,50
1,70
1,90
ml
1 : 2.5
1 : 0.5
Atg8
Atg19 C-terminus

B

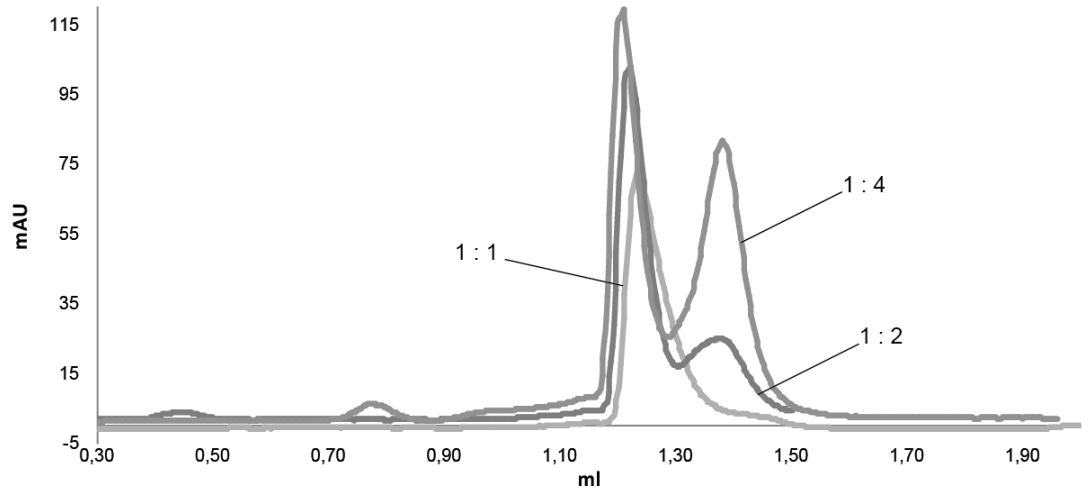
115
95
75
55
35
15
-5
mAU
0,30
0,50
0,70
0,90
1,10
1,30
1,50
1,70
1,90
ml
1 : 4
1 : 1
1 : 2

C

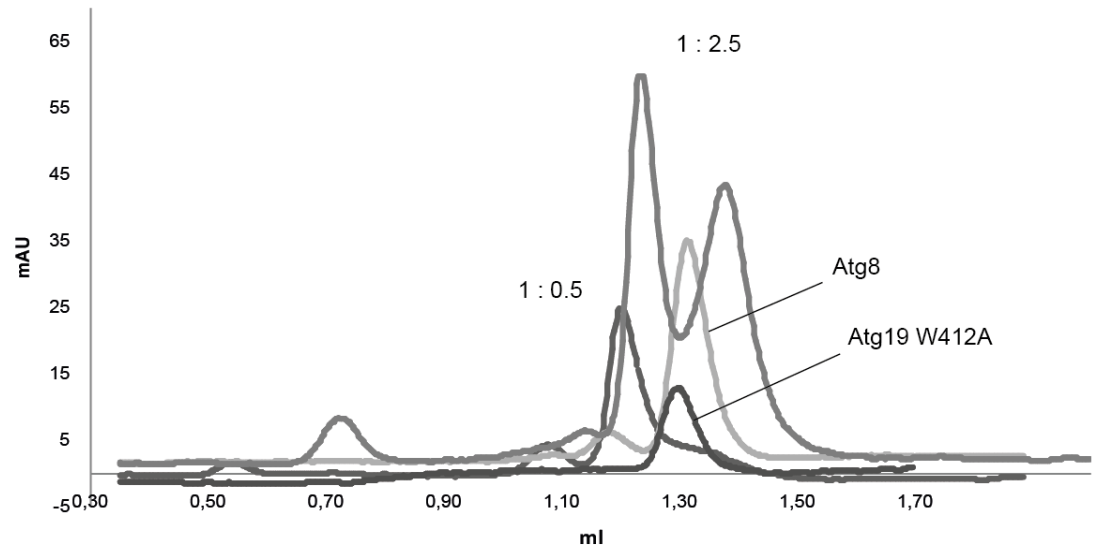
65
55
45
35
25
15
5
-5
mAU
0,30
0,50
0,70
0,90
1,10
1,30
1,50
1,70
ml
1 : 2.5
1 : 0.5
Atg8
Atg19 W412A

D

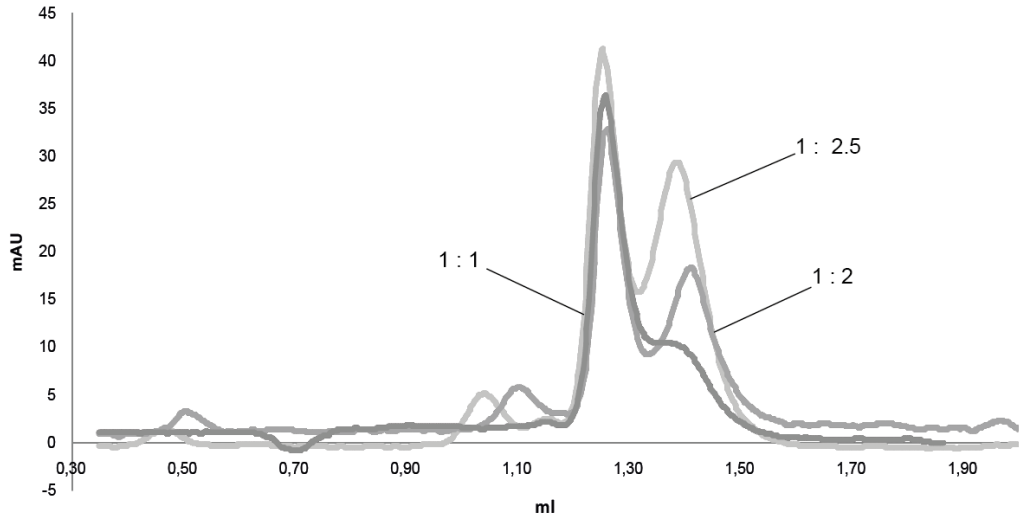

Figure 15: Overlayed280 nm-absorption profiles in size exclusion chromatography of Atg19 C-terminal domain and Atg8 (previous page)
Purified Atg19 aa365-415 wild type (A and B) or W412A mutant (C and D)kept constant at 40 µM was mixed with purified Atg8 at 20 – 160 µM (ratios as indicated) and subjected to high pressure liquid chromatography on an Ettan HPLC system using a Sepharose75 32/30 column. Tested molar ratios: 1: 0.5 to 1: 2.5. (A) Atg8 and Atg19 C-terminal domain alone at 40 µM respectively and mixed in a molar ratio of 1 : 0.5 and 1: 2.5. (B) Atg19 C-terminal domain in fixed concentration of 40 µM mixed with Atg8 in increasing concentrations (as indicated). (C) Atg8 and Atg19 C-terminal domain W412A at 40 µM respectively and mixed in a molar ratio of 1 : 0.5 and 1: 2.5. (D) Atg19 C-terminal domain W412A in fixed concentration of 40 µM mixed with Atg8 in increasing concentrations (as indicated).The UV-absorption peak of the complex of Atg19 C-terminus and Atg8 is recorded at ca 1.2 ml, UV-absorption peak of unbound Atg8 is at about 1.4 ml. Representative curves for each experiment are shown.

Analytical size exclusion chromatography to calculate the number of bound Atg8 molecules per one molecule of Atg19's C-terminal domain

The purified Atg19 C-terminal domain in different mutant versions (F376A, F379A; W412A; F376A, F379A, W412A) was incubated with purified Atg8 for 30 minutes at 4°C in a molar ratio of 40 µM (Atg19 C-terminus) to 400 µM (Atg8). This complexation reaction was analyzed in size exclusion chromatography using a Sepharose200 10/300 column on an Äkta purifier system. From these experiments the number of bound molecules of Atg8 to one molecule of Atg19 aa(365-415) wild type; W412A or F376A, F379A, W412A was calculated.. The retention volumes and the UV-absorption peaks of Atg19, Atg8 and complex thereof were recorded using the UNICORN software. Atg19 C-terminal domains were retained until approximately 16.1 to 16.2 ml, Atg8 until approximately 17.2 ml and the complex of these two to approximately 15.9 ml (see Table 4 and Figure 16).

Recombinant protein	Retention volume FPLC	Concentration	Extinction coefficient
Atg19 aa365-415	16,1-16,2	40 µM	8480
Atg19 aa365-415 W412A	16,1-16,2	40 µM	2980
Atg19 aa365-415 F376A, F379A, W412A	16,1-16,2	40 µM	2980
Atg8	17,2	400 µM	8940
Atg19 aa365-415-Atg8 complex	15,78		
Atg19 aa365-415 W412A-Atg8 complex	15,96		
Atg19 aa365-415 F376A, F379A, W412A-Atg8 complex	16,3		

Table 4: Retention volumes of Atg19 C-termini, Atg8 and the complex of these on an Äkta purifier system using an S200 10/300

The number of bound molecules of Atg8 per molecule of Atg19 C-terminus was calculated by integrating the peaks of the absorption-profile corresponding to the respective protein or protein complex, that is Atg19 C-terminus alone, Atg8 alone or the complex thereof. Then, the integral of the absorption peak of Atg19 C-terminus alone run at 40 µM was subtracted from the integral of the Atg19 C-terminal domain-Atg8 complex peak in a ratio of 40:400 µM (Atg19 C-terminus:Atg8). The difference represents the amount of Atg8 in complex with Atg19 C-terminus. Relating this value to the integral of Atg8 run alone at 400 µM and multiplying this ratio by the working concentration of Atg8 (400µM) gives the concentration of Atg8 shifted into the complex peak. This value was finally divided by the concentration of Atg19 C-terminus used in the reaction (40µM) to obtain a value for the number of Atg8 molecules complexed by one Atg19 C-terminus (see Figure 16).

Calculation:

$\int$ complex – $\int$ C-terminus control = Atg8 in complex with Atg19 C-terminus

$\int$ complexed Atg8 / $\int$ Atg8 run alone x c[Atg8] = c[complexed Atg8]

c[complexed Atg8] / c[Atg19 C-terminus] = number of Atg8 per Atg19 C-terminal domain.

For Atg19 aa(365-415) wild type at 40 µM complexed with Atg8 at 400 µM a binding capacity of four (mean of three experiments = 4.14) molecules of Atg8 was calculated.

Atg19 aa(365-415) W412A is predicted to bind two (mean of three experiments = 1.81) molecules of Atg8 and also Atg19 aa(365-415) F376A, F379A, W412A interacts with two (mean of three experiments = 2.19) molecules of Atg8 (Figure 16). This higher number of the

triple mutant compared to the W412A only mutant might be due to the transient nature of the interaction or to slight experimental deviations.

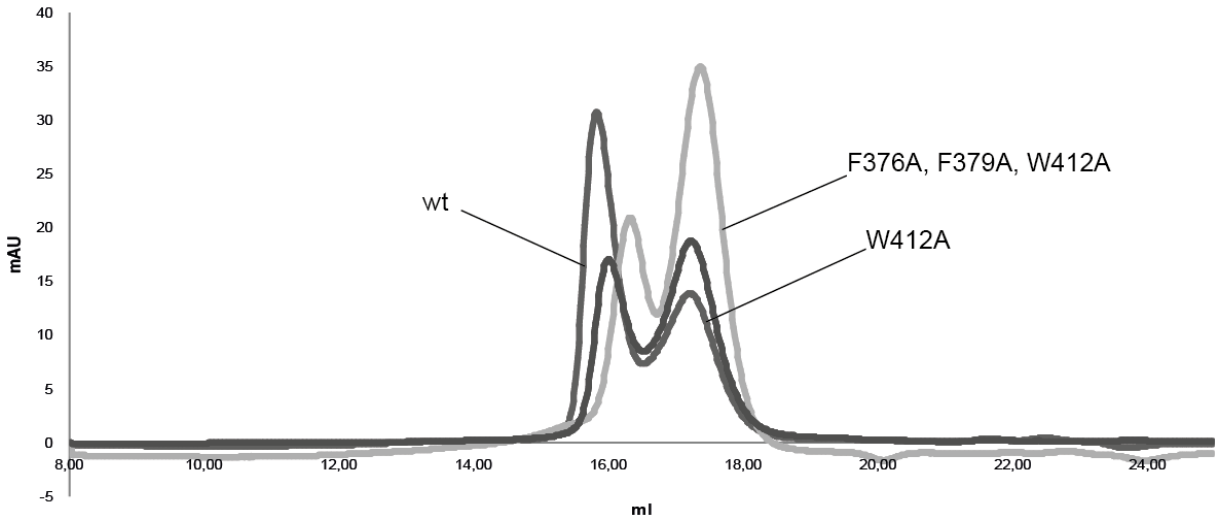

Figure 16: Overlayed280 nm-absorption profiles in size exclusion chromatography of Atg19 C-terminal domain mutants and Atg8 at a molar ratio of 1:10
Purified Atg19 aa365-415 wild type, W412A mutant or F376A, F379A, W412A mutant (as indicated)at 40 µM was mixed with purified Atg8 at 400 µM and subjected to high pressure liquid chromatography on an Äkta purifier FPLC system using a Sepharose 75 10/300 column. The UV-absorption peak of the complex of Atg19 C-terminus and Atg8 is recorded at ca 15.9 ml, UV-absorption peak of unbound Atg8 is at ca 17.2 ml. Representative curves for each experiment are shown.

Efficiency of cargo delivery to giant unilamellar vesicles of recombinant Atg19 versions

Atg19 serves as a cargo receptor for the vacuolar hydrolase prApe1 in *Saccharomyces cervisiae* linking the cargo by the autophagic membrane. Previously conducted *in vivo* experiments suggested that multiple Atg8 binding sites in Atg19 are required for the Cvt pathway where the isolation membrane is tightly wrapped around the prApe1 cargo. In addition experiments showed that Atg19 is able to tightly bend Atg8-positive membranes around prApe1 cargo mimetic microspheres. In order to further examine if the multiple Atg8 binding sites in Atg19 are required for this activity they were assessed microscopically using giant unilamellar vesicles (GUVs). A spinning disc microscope was used to visualize the lipid dye Rhodamine (red) at a wavelength of 561 nm, green fluorescent protein (*GFP*, 488 nm, green) and differential interference contrast. The vesicles of a diameter of approximately 5–100 µm were generated by applying a current to an ITO coated glass plate covered with vacuum-dried lipid droplets. The lipid mixes contained 5-25% DGS-NTA and 85% POPC fluorescently labeled for microscopy with the red dye rhodamine. DGS-NTA was used to bind 6xhistidine-tagged Atg8 to mimic the *in vivo* situation where Atg8 is covalently bound to the head groups of the membrane lipid phosphatidylethanolamine. Latex beads of a diameter of 2 µm (Invitrogen) coated with recombinant monomeric enhanced GFP fused prApe1-propeptide were used to represent the enzymatic cargo of the Cvt-pathway.

In the experimental set up, purified Atg19 protein either in wild type or in different mutant versions was incubated with prApe1-propeptide-beads. After incubation of C-terminally 6xHis-tagged Atg8 with the GUVs, these beads were added to the Atg8 coated GUVs. Atg19 on the beads interacts with Atg8 on the GUVs and if this interaction is strong enough, the membrane will bend around the bead (see Figure 17).

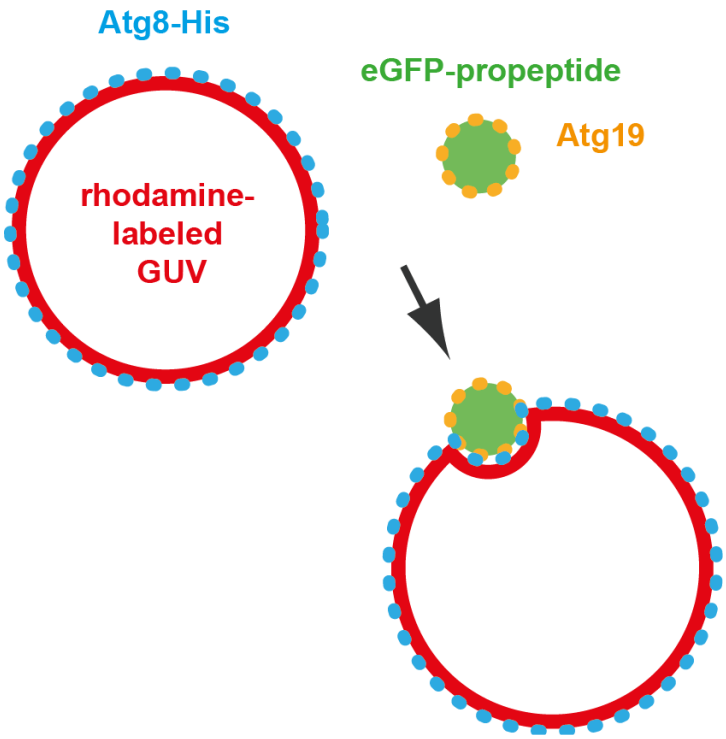

Figure 17: Experimental set-up to assess membrane bending of Atg8-covered GUVs conferred by Atg19 and prApe1-propeptide on beads
Atg8 (blue) is attached to the rhodamine labeled GUV (red) via interaction of its 6xHis-tag and the Nickel-lipids. Atg19 (orange) binds to the latex bead (green, represents Cvt-cargo) via cross-linked mEGFP-prApe1-propeptide. When GUVs and beads are mixed, Atg19 and Atg8 interact resulting in partial engulfment of the bead.

The capacity to bend the GUV-membrane of various Atg19-mutants was assessed. In every experiment two controls were set up. These contained either wild type Atg19 (positive control) or no Atg19 protein (only buffer, negative control). A bending event was assumed when the rhodamine-labeled GUV-membrane was clearly seen around the 2 µm-shape of a mEGFP-propeptide coated latex bead, comparing the 488 nm and the 561 nm channel of the spinning disc microscope(compare in Figure 18: upper panel (no bending without the receptor) and lower panel (wt bends the vesicle)).

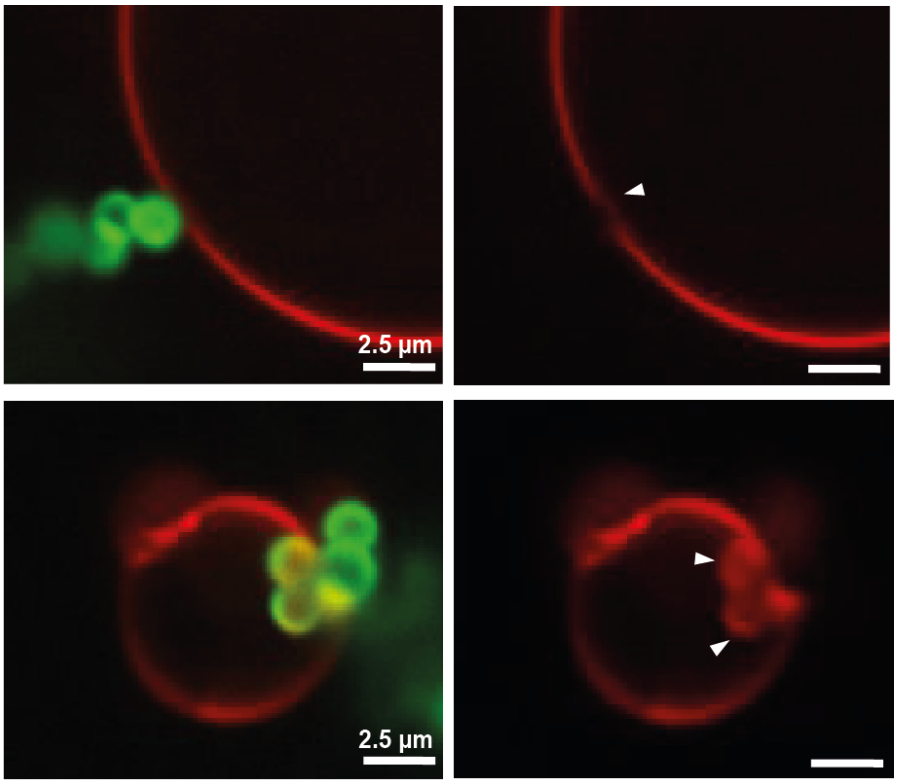

Figure 18: GUV assay to quantify the membrane bending qualities of Atg19.
GUVs were fluorescently labeled in red using rhodamine-dye. Atg8-His was attached to the vesicle membrane via Ni-containing lipids (DGS-NTA). Bending of the membrane by latex beads coated with mEGFP-prApe1-propeptide was assessed in fluorescence microscopy. Left: overlay of 488 nm and 561 nm signals (GUV and mEGFP-propeptide-coated beads). Right: 561 nm signal (GUV).
Upper panel: no Atg19 added to the reaction. Lower panel: Atg19 wild type.

The tested Atg19 versions were wild type, Atg19 W412A (canonical LIR-mutant), Atg19 F376A, F379A (cryptic LIR-mutant), Atg19 F376A, F379A, W412A (both LIR motifs mutated) and a chimerical version of the two Cvt-receptors Atg19 and Atg34 that consisting of the N-terminus (aa1-364) of Atg19 and the C-terminus aa(367-412) of Atg34. The Atg19-Atg34 chimeric protein contained only one LIR motif (aa409-412), i.e. the LIR motif in the C-terminus of Atg34 (aa409-412) and in contrast to Atg19no additional Atg8-interaction sites. Bending events were counted examining propeptide-coated beads associating with GUVs, i.e. beads that are overlapping with GUV-membranes. As a control no recombinant Atg19, but buffer was added to a sample of beads that were otherwise treated the same way. Percentages were calculated by relating bending events to association events.

An average of 79% from three independent experiments of wild type Atg19-bound beads lead to bending of GUV-membranes (arrowheads, Figure 18, lower panel). 25% of prApe1-propeptide coated beads incubated without any Atg19 introduced a curvature in the GUV-membrane. In three independent experiments 42% of Atg19 W412A mutant-bound beads were curving GUV-surfaces, whereas 52% of F376A, F379A mutants did the same. When

both Atg8-binding sites were silenced by mutating the respective amino acids to alanine only 35% of the Atg19 mutant coated beads were able to bend the GUV membrane around them. Changing both P385 and E386 to A additionally to the F376A, F379A and W412A-mutations reduced the bending capacity of Atg19 to 28%. The Atg19-Atg34 chimeric protein as receptor showed a membrane bending capacity of 66% (Figure 19 and 20).

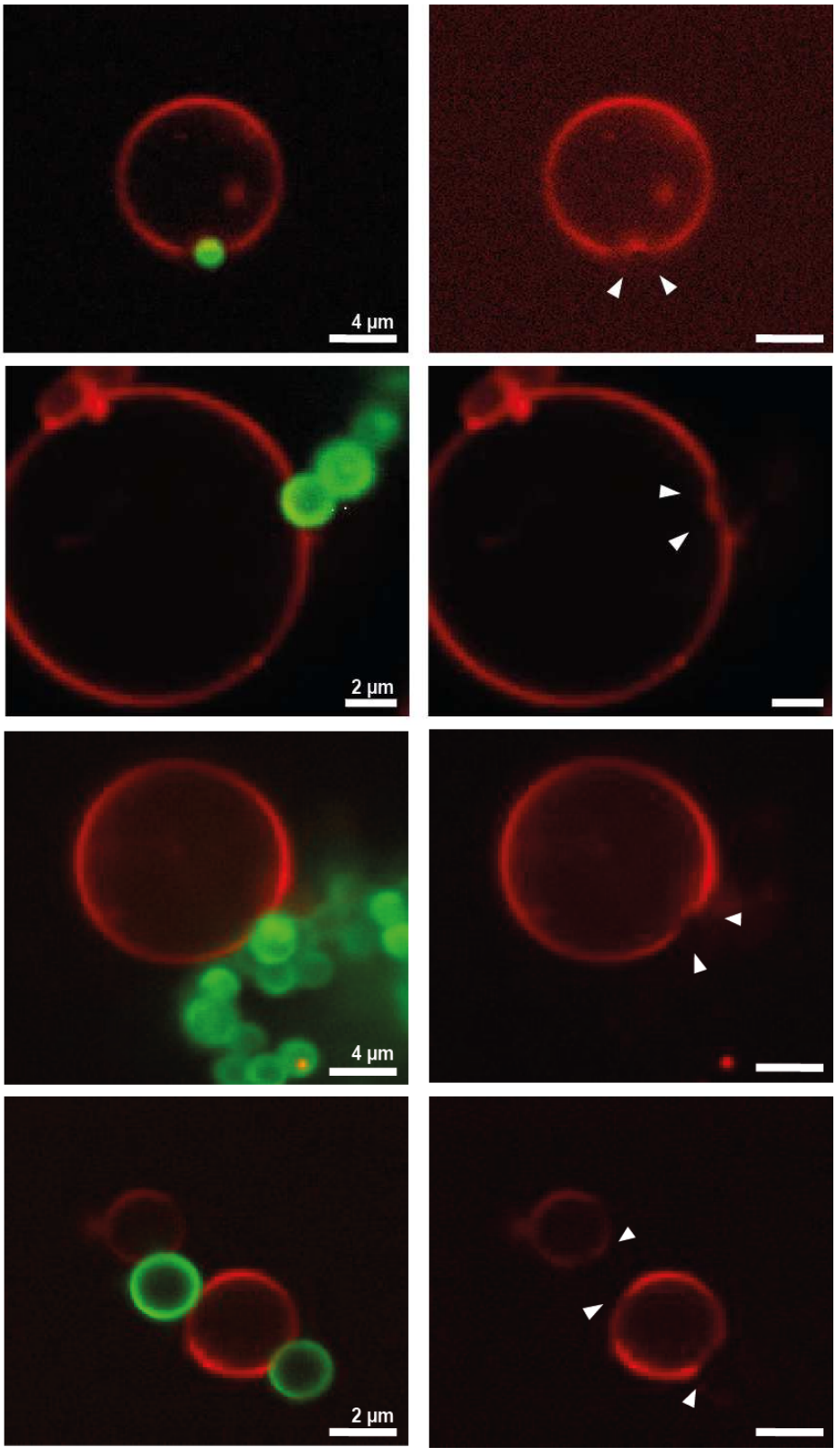

Figure 19: GUV assay to quantify the membrane bending qualities of Atg19 mutants (previous page).
GUVs were fluorescently labeled in red using rhodamine dye. Atg8-His was attached to the vesicle membrane via Ni-containing lipids (DGS-NTA). Bending of the membrane by latex beads coated with mEGFP-prApe1-propeptide was assessed in fluorescence microscopy. Left: overlay of 488 nm and 561 nm signals (GUV and mEGFP-propeptide-coated beads). Right: 561 nm signal (GUV).
First panel: Atg19 W412A mutant. Second panel: Atg19 F376A, F379A mutant. Third panel: Atg19 F376A, F379A, W412A mutant. Fourth panel: Atg19 F376A, F379A, P385A, E386A, W412A mutant. Scale bars for each Atg19 mutant respectively.

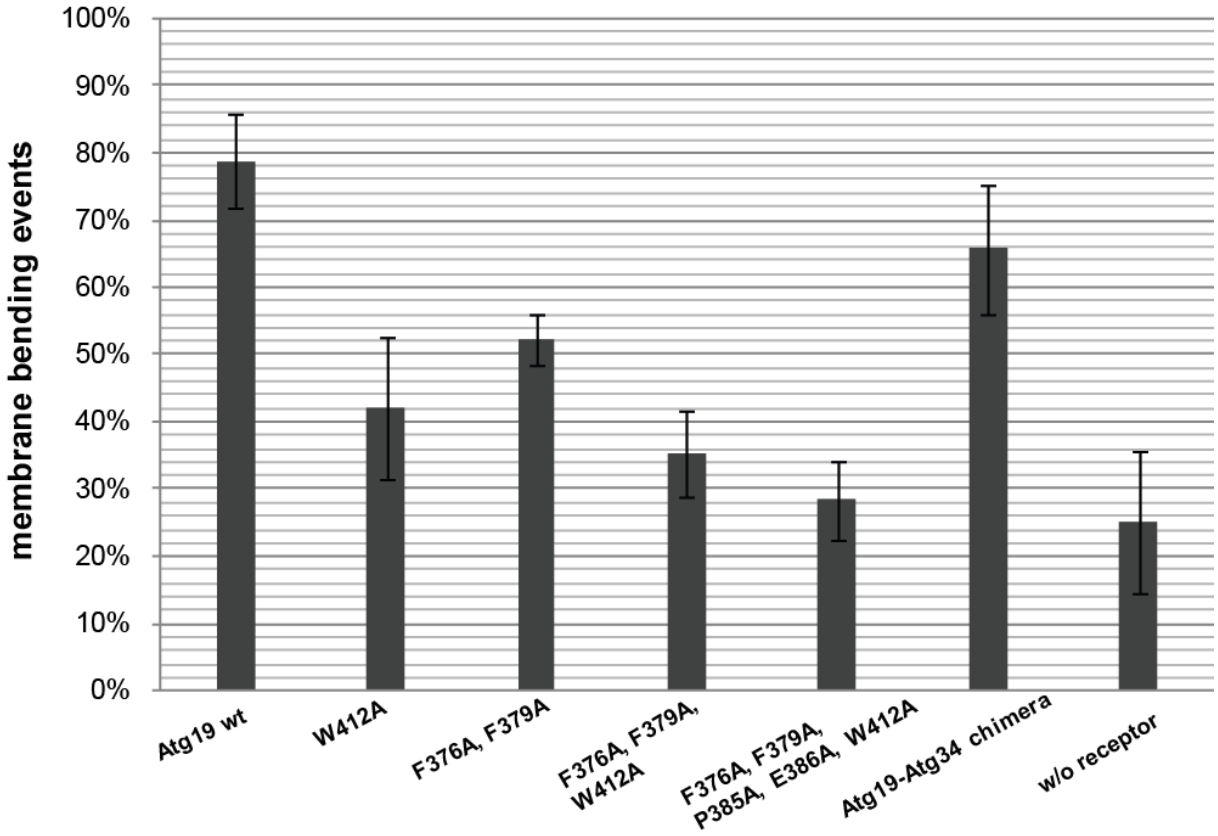

Figure 20: Quantification of membrane bending conferred by different Atg19 mutants.
Membrane bending events of GFP-prApe1 coated latex beads associated to GUVs were counted in 3 independent experiments. y-axis: Percentage of membrane bending of the respective Atg19 mutant, 100%: counted events of association of beads and GUVs. x-axis: Atg19 mutants.

Influence of Atg8-coverage of the membrane on cargo delivery

The results shown in the previous paragraph strongly suggest that the ability of Atg19 to bend the Atg8-positive GUV membrane around the cargo mimetic beads positively correlates with number of Atg8 binding sites in its C-terminus. In order corroborate these findings the density of Atg8 on the GUV membrane was titrated. If membrane bending is a function of the number of Atg8-Atg18 interactions, then membrane bending should decrease of the density of Atg8 on the membrane is reduced. The density of Atg8 on the membrane was controlled by changing the amount of DGS-NTA (Nickel containing lipids) lipid mixes used for GUV preparation. Since Atg8-His binds to the nickel on the GUV membranes, Atg8 coverage of the

membrane can be inferred from the amount of nickel in the membrane. Bending was assessed the same way as in previous experiments. Representative pictures are shown in Figure 21. Nickel concentrations on the GUV membranes ranged from 1% to 25%. Every concentration was tested in three independent experiments, the number of counted events per experiment varied from 5 to 25. 15% Ni-lipids lead to membrane bending in 70% of counted events confirming the results of previous experiments (see Figure 18 and 19). Increasing the DGS-NTA concentration to 25% did not seem to influence the bending efficiency (69%) possibly because the membrane is already saturated with Atg8 at 15% Ni-lipids. In contrast, a decrease to 5% nickel resulted in only 49% of bending events per counted membrane-bound beads. Therefore the Ni-lipids were diluted further to 2.5% and 1 %. Here 19% and 14% of bending events respectively were counted (Figure 21 and 22) indicating that at least 5% Atg8 coverage of the membrane is necessary for cargo enwrapment. Interestingly, even though some bending was visible in 5% nickel membranes, the extent of bending was generally lower compared to higher concentrations (Figure 21).

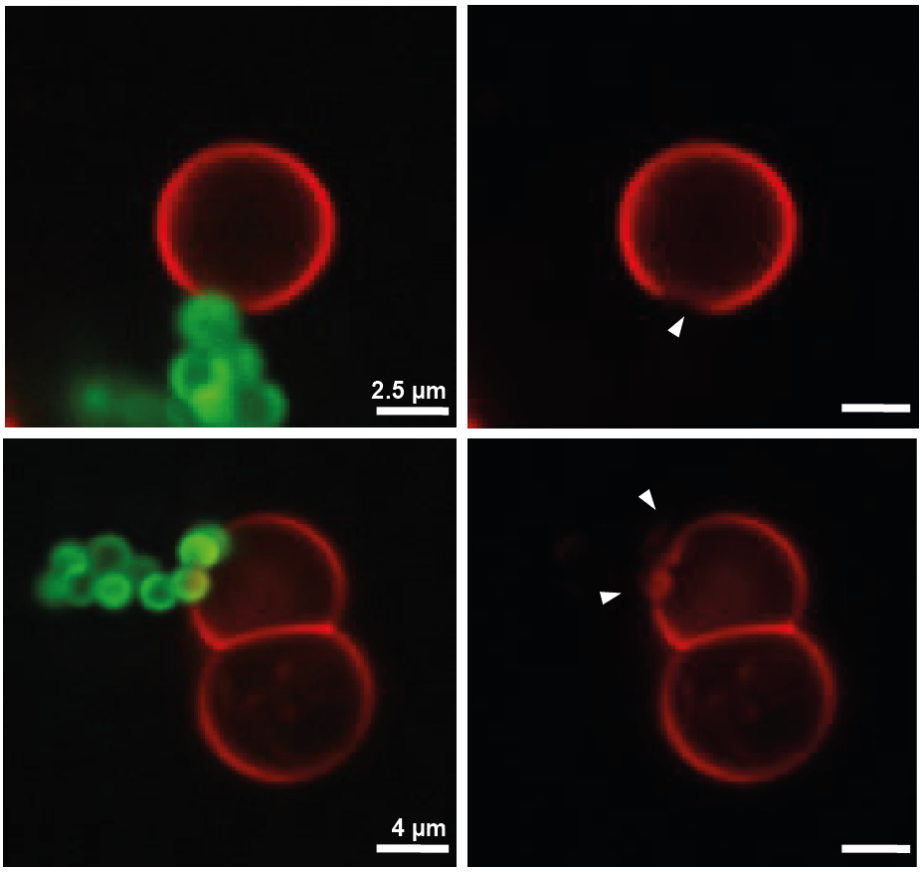

Figure 21: GUV assay to quantify the membrane bending qualities of Atg19 at different Ni-concentrations.
GUVs were fluorescently labeled in red using rhodamine-dye. Atg8-His was attached to the vesicle membrane via Ni-containing lipids (DGS-NTA). Bending of the membrane by latex beads coated with mEGFP-prApe1-propeptide was assessed in fluorescence microscopy. Left: overlay of 488 nm and 561 nm signals (GUV and mEGFP-propeptide-coated beads). Right: 561 nm signal (GUV).
First panel: GUVs prepared with 1% DGS-NTA. Second panel: GUVs prepared with 5% DGS-NTA.

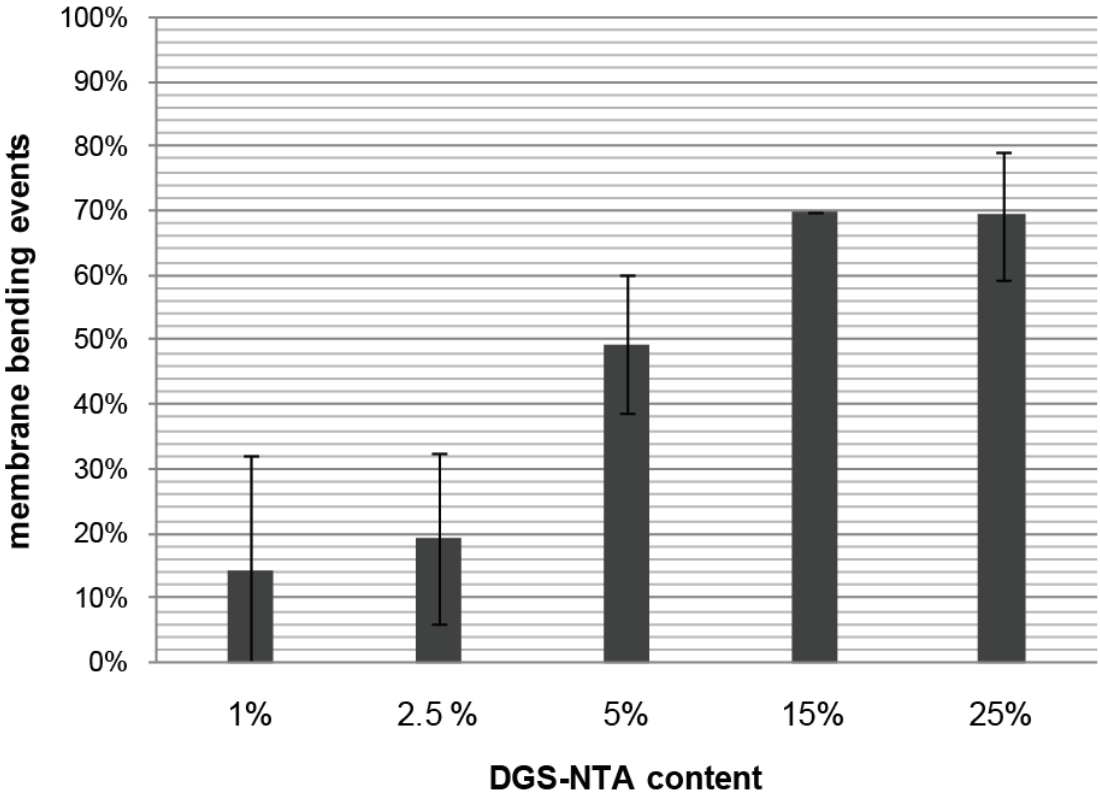

Figure 22: Quantification of membrane bending conferred by Atg19 at different Ni concentrations.
GUV Membrane bending events of GFP-prApe1 coated latex beads associated to GUVs were counted in 3 independent experiments. y-axis: Percentage of membrane bending of the respective DGS-NTA concentration of the GUVs, 100%: counted events of association of beads and GUVs. x-axis: DGS-NTA concentration in GUVs.

IV Discussion

This thesis provides a deeper insight into the molecular mechanisms underlying the interaction of the yeast autophagy receptor Atg19 and the membrane associated protein Atg8. During the Cytoplasm-to-vacuole targeting (Cvt) pathway Atg19 interacts simultaneously with its cargos Ams1 and prApe1 (via its propeptide of 45 aa)[59] and PE-conjugated Atg8 that resides on the isolation membrane[32,48]. This activity serves to connect the multimeric cargo complex to the site of Cvt-vesicle formation. On one side Atg19 binds the cargo and on the other it indirectly binds the forming autophagic membrane (by Atg8) thus pulling these two together so that the cargo can finally be enwrapped by the membrane and subsequently be delivered to the vacuole to be degraded. The conducted *in vitro* experiments show that there are more Atg8-interaction sites in Atg19 apart from the previously known LIR-motif WEEL[52].

Pull-down experiments using recombinant Atg8 and truncated Atg19 versions revealed that there might be more than one Atg8 interaction site in the molecule. The C-terminal domain of Atg19 (aa365-415) seemed to interact stronger with Atg8 than the full length molecule, suggesting a potential self inhibition of the receptor (compare Figure 9 (A) and (B), (C)). Atg19 with a truncated C-terminus. i. e. missing the LIR-motif (the only known Atg8 interaction site in Atg19 so far) located at position 412-415 was still able to interact with Atg8 in these experiments. Atg19 aa1-374, aa1-384 and aa1-396 interacted with Atg8 in GST-fused versions with untagged Atg8 as well as in the vice-versa situation using untagged Atg19 and a GST-Atg8. In addition, Atg19 mutants with a mutated LIR (W412A-mutation) and truncated from the N-terminus, namely Atg19 aa376-415 WA and aa386-415 WA were still able to bind Atg8. The strength of the Atg19-Atg8 interaction judged by Western Blot decreased the longer the truncated sequence (from the N-terminus or the C-terminus) of Atg19 was. But t
he Atg19 constructs that were truncated from the N-terminus bound more Atg8 than the longer constructs that were missing the C-terminus. In experiments using the aa398-415 WA mutant and Atg8, no bound Atg8 could be detected, indicating that C-terminally from aa 398, the only Atg8 interaction site is the LIR motif, whereas there must be additional interaction sites in C-terminal domain. Since Atg19 aa1-374 bound Atg8, there might be one N-terminally of aa 374. However, this interaction might be rather weak. Atg19 aa 1-384 also bound Atg8 and in a stronger manner compared to aa1-374. Extending the C-terminus to include aa1-396 further increased Atg8 interaction (Figure 9(C)). This suggests that there might be one Atg8 interaction site between aa374 and aa384 as well as another one between

aa384 and aa396. The behavior of the C-terminal constructs truncated from the N-terminus corroborated these findings. Atg19 aa376-415 bearing the LIR motif silencing mutation W412A interacted strongest with Atg8 in pull down experiments. Atg19 aa386-415 W412A showed decreased binding of Atg8 and the aa398-415 W412A protein failed to interact with Atg8 (Figure 9 (C)). These results were also confirmed using GST-fused Atg8 (Figure 9 (D)).
Starting from these results, potential interaction sites in Atg19 were point-mutated to pin down the exact location of additional Atg8 interactions in another set of GST-pull-down experiments.
Using recombinant Atg8 and Atg19 mutants revealed that aa376-379 (motif FYSY-) may be one of these additional Atg8 interaction sites, since a mutation of F376 and F379 to alanines reduced binding of Atg8, which was even more evident in a W412A (LIR) mutant background (see Figure 12). This FYSF-motif strongly resembles LIR motifs found in other autophagy receptors, like for example an FVEI sequence in the mammalian receptor optineurin[68]. Phenylalanine is hydrophobic similar to tryptophan and leucine in the more common WxxL LIR motif. Another hint to FYSF being a LIR motif would be that mutating F376 (at the first position of the sequence) has a more negative effect on the amount of bound Atg8 in pull down experiments than mutation of F379 (at the fourth position). Analogous results have been published for Atg19's WEEL motif 52.
Furthermore, a PE-motif at aa 385 and 386 might play a role in binding Atg8. This sequence upstream of the known Atg11 binding site is conserved in the mammalian autophagy receptor p62 (Figure 11). Mutating this motif to A also resulted in decreased Atg8-binding in a LIR-mutant background (Figure 13). When all three of the mentioned sites, i.e. F376, F379, P384, E385 and W412 where mutated to A simultaneously the interaction of Atg19 with Atg8 was severely decreased (Figure 13). These results were also confirmed using GST-fused prApe1 propeptide (Figure 14). This set-up is the best model of the *in vivo* situation. Just like the Cvt complex in the cell, the GSH bead contains the GST-fused prApe1 propeptide highly concentrated on its surface. Atg19 binds to this particle via its coiled coil domain as well as to Atg8.
The pull down experiments discussed above strongly suggested that Atg19 has multiple Atg8 interaction sites. In order to test if Atg19 has the ability to interact with multiple Atg8 molecules simultaneously size exclusion chromatography experiments with an excess of Atg8 over Atg19 were conducted. The Atg19 C-terminal domain in wt and the F376A, F379A, the W412A and the F376A, F379A, W412A mutant versions were subsequently subjected to size exclusion chromatography to shed light on the stoichiometry of Atg8 binding. The C-terminal

domain was used because it was observed to bind stronger to Atg8 than the full-length molecule and to omit experimental complications due to the assumed inhibitory activity of the coiled-coil domain. First, Atg19 wt and W412A were mixed with Atg8 in different molar ratios to get an estimate of the amount of Atg8 that can be taken up by Atg19' C-terminus. The molar ratios ranged from 1: 0.5 to 1:4 and 1:2.5 for the wt Atg19 C-terminus to Atg8 and the W412A mutant to Atg8 respectively, i.e. 40 µM Atg19 C-terminus : 20 µM Atg8 to 160 µM Atg8 or 100 µM Atg8 (W412A mutant). The tested titration concentrations differ, because for the W412A mutant a saturation was observed at a ratio of 1: 2.5 (corresponds to 100 µM Atg8, Atg19 C-terminus:Atg8). The binding capacity of Atg19 C-terminus to Atg8 was assessed by observing the UV peaks of the Atg19 C-terminus-Atg8 complex and the Atg8 peak (Figure 15). The more Atg8 is added to the reaction the more will be bound to the complex, until a saturation point is reached, indicated by the appearance of a second UV absorption peak recorded at the same retention volume as observed for Atg8 alone in a control run. At a ratio of 1:4 of Atg19 wt C-terminus to Atg8, the UV-profile of the gel filtration indicated a saturation of Atg19 suggesting that Atg19 binds four molecules of Atg8 (Figure 15). For the W412A mutant this ratio of saturation was between 1:2 and 1:2.5, which indicated that this mutant might only bind two or three molecules of Atg8 in vitro. To obtain more insights into the binding stoichiometry, size exclusion chromatography was conducted with Atg19 C-terminus in wt, W412A mutant and F376A, F379A, W412A mutant versions in fixed ratios of 1:10 of Atg19 to Atg8. In this series of experiments the amount of bound Atg8 was calculated from the UV-absorption profiles of the gel filtration runs. Each wild type Atg19 bound on average (of three independent experiments) four molecules of Atg8. Atg19 W412A bound on average 2 molecules of Atg8 and also Atg19 F376A, F379A, W412A two molecules on average (Figure 16).

The hypothesis that the reduced binding capacities of Atg19 mutants have an effect on the specificity of cargo delivery during Cytoplasm-to-vacuole targeting was tested applying a model to mimic cargo binding and membrane enwrapment *in vitro.* The question addressed here is, if Atg19-Atg8 interaction is important for tightly wrapping the autophagic membrane around cargo proteins 2 µm-latex beads cross-linked to prApe1-propeptide (aa1-45) fused to GFP were incubated with recombinant Atg19 versions to allow binding of the receptor (Atg19) to the cargo (prApe1-propeptide) and then mixed with giant unilamellar vesicles covered with 6xHis-tagged Atg8. The propeptide-covered beads will bind Atg19 on their surface, assuming a functional interaction of these two proteins[59,60]. Atg19 on the other hand also binds to Atg8 and by this linking activity the beads representing the autophagic cargo

will come close to the Atg8-containing membrane. If the interaction of the receptor and Atg8 is strong enough the membrane will be bent around the cargo. Consequently, the more Atg8 binding sites there are on Atg19, the stronger the interaction will be and hence the bending activity will be increased. Membrane bending events were quantified for Atg19 in wild type, the W412A mutant, the F376A, F379A double mutant, the W412A, F376A, F379A triple and the quintuple W412A, F376A, F379A, P385A, E386A mutants.

The results point to a show that membrane bending positively correlates with the number of potential Atg8 binding sites. With Atg19 wild type 78% of beads associated to vesicles induced a bending of the membrane around the bead, whereas in a W412A background only 42% did so. A chimeric protein consisting of the N-terminal part of Atg19 and the C-terminus of Atg34 where the LIR was silenced by mutating W409 to Ala, was able to bend the membrane in 66% of observed beads-to membrane association. In a F376A, F379A background 52% of associated beads elicited a curving of the membrane and 35% did so when the LIR was silenced in this background. Again, the effect was most drastic in the quintuple mutant, where three (potential) binding sites were rendered nonfunctional. Here only 28% of Atg19-mutant-bound propeptide beads lead to a deformation of the membrane (Figure 18-20). Since a decrease in Atg8 on the membrane, brought about by reducing the Ni content to 1-5% (Figure 21 and 22), a high concentration of Atg8 on autophagic membranes is also important in efficient cargo delivery. The presented results strongly suggest that the strength of Atg19-Atg8 interaction brought about by the number of interaction sited on Atg19 is important for the efficient cargo delivery to autophagic membranes. Simultaneously these observations were corroborated by *in vivo* experiments assessing the efficiency of Ape1 maturation in *S. cervisiae* strains expressing the respective Atg19 mutant.

Taken together, the experiments conducted for this thesis suggest that apart from the previously known Atg8 binding site in the Cvt cargo receptor Atg19, there might be at least four more. It is likely that some of these reside in the C-terminal domain of Atg19, since this part alone showed a stronger interaction with Atg8 than the full-length molecule (Figure 9, JSM). This has interesting implications for a model of cargo recognition by the receptor. The binding of prApe1 occurs N-terminally (aa124-254) whereas the linkage to the membrane via Atg8 apparently happens in the C-terminal region of Atg19. Suggesting that the C-terminus serves as an interface that connects the Cvt-vesicle to the autophagic membrane forming machinery. Therefore Atg8 interaction sites are concentrated in the C-terminus inducing multiple binding. This might be required for specific binding of the autophagic membrane, on which Atg8 is concentrated. If Atg19 contained a high affinity binding site (as opposed to

high avidity), interaction of the receptor and Atg8 might also occur in solution, which would be counteracting selective cargo sequestration. Each of the single Atg8 binding sites in Atg19 has probably a relatively low affinity and only if an array of them comes to the site where the interactor Atg8 is highly concentrated (i.e. the 2-dimesional surface of the isolation membrane), strong binding and consequently selectivity is ensured.

One of the potential Atg8 binding sites was identified as a FYSF sequence in the C-terminal domain of Atg19. This motif has as mentioned strong similarities with known Atg8-interacting LIR motifs. The conducted experiments also clearly show an involvement of this amino acid stretch in Atg8 binding. FYSF may be another LIR motif in Atg19 besides the C-terminal WEEL sequence. It is not conserved in the Cvt receptor Atg34, which is known to have only one Atg8 interaction site in its C-terminal region (W409EEI, Figure 11, JSM)[51]. FYSF may be another LIR motif in Atg19 besides the C-terminal WEEL sequence.

Another site involved in Atg8 binding might be a PE motif directly N-terminal of the interaction site with the Cvt-specific scaffold protein Atg11. Experimental results have shown that these two amino acids might be involved in Atg8 interaction, since mutating them to alanines lead to a decrease of bound Atg8 detected in pull downs in a LIR-mutant background. If these residues are directly binding to Atg8 is not clear, it might be possible that exchanging the rather big ring-structured proline as well as an acidic glutamate for the small non-polar amino acid alanine interferes with the structure of Atg19. This might impair accessibility of the Atg8 binding sites. On the other hand, the close proximity of these functional sequences (i.e. the Atg11 binding site and an Atg8 binding site) hints to an interplay between different Cvt-factors in cargo delivery. It might be possible that Atg19 first binds Atg11. This interaction could bring the Cvt complex (Atg19 bound to the prApe1 aggregate) to the site of Cvt vesicle formation. Once there, tethering via Atg11 is not necessary anymore, but instead membrane enwrapment of the Cvt complex is induced. This would be conferred by interaction of Atg19 with membrane bound Atg8. So first the Atg11 binding site in Atg19 would be occupied and subsequently Atg8 binding removes Atg11 from the Cvt complex by steric constraints. Prerequisite for this model would be a stronger binding of Atg19 to Atg8 than to Atg11. This might easily be possible keeping in mind that there is one Atg11 interaction site and several Atg8 interaction sites in Atg19. This motif could serve as a regulatory site for switching from binding of the receptor to the Cvt-scaffold Atg11 to the membrane-bound Atg8 thus functioning at the intersect of Cvt complex assembly to vesicle formation.

In future studies it would be interesting to resolve a structure of the complex of Atg19 C-terminus in different mutant versions and Atg8. By comparing the structures of the wild type and the LIR (W412A) mutant of Atg19 C-terminus, the binding mechanisms of other Atg8 binding sites apart from the LIR motif could be elucidated. Since Atg8 might interact at different sites in a rather transient manner with Atg19 C-terminus, nuclear magnetic resonance spectroscopy might be rather applicable that X-ray crystallography, where one species of molecules would be required to gain an ordered protein crystal. But if Atg19 and Atg8 interact via various sites, there might be several different complex molecules in solution.
Another focus of investigation could be previously observed Atg8 binding enhancement upon addition of the prApe1 propeptide to interaction experiments (see introduction). This effect could result from a self inhibition of Atg19, possibly conferred by the prApe1 propeptide binding site in the coiled coil domain of Atg19. The inhibition could be released by binding of the cargo. The interaction might lead to some conformational change of Atg19 that exposes additional Atg8 binding sites. Preliminary experiments probing for Atg19 self interaction did not show any positive results. But the applied experimental set up can be improved to gain reliable results. Recombinant Atg19 domains (N-terminus, cc-domain containing the prApe1 propeptide binding site, Ams1-binding domain and C-terminus) were tested for interaction in GST-affinity pull downs which were analyzed by SDS-PAGE and subsequent CBB staining. Possible interactions might be too weak to be detected on a CBB gel. Western blotting with an antibody raised against Atg19 could solve this problem.
A third interesting point of research would be the interplay of Atg19's interaction with the Cvt scaffold protein Atg11 on one hand and the interaction with Atg8 on the other. Atg11 is responsible for bringing the Atg19-cargo complex to the PAS. Considering this, it is well conceivable that the interactions of Atg19 with Atg8 and Atg11 have an influence on each other. First the Cvt complex, that is Atg19, has to bind to Atg11 to be transported to the PAS. Once there, Atg11 binding is not required anymore, but connecting the Cvt-complex to lapidated Atg8 on the autophagic membrane is necessary to form the Cvt vesicle. So in vitro pull downs binding Atg11 to GST-Atg19 on GSH beads, addition of Atg8 might weaken this interaction. By including Atg11 to the GUV experiment-set up could result in changed dynamics of cargo-membrane association or membrane bending.
Understanding the molecular mechanisms underlying selective autophagy in yeast will provide a model for similar pathways in higher eukaryotes, which are known to be involved in clearance of various potentially dangerous agents, such as damaged cellular organelles, bacteria and viruses and aggregated protein.

References

1 Birmingham, C. L., Smith, A. C., Bakowski, M. A., Yoshimori, T. & Brumell, J. H. Autophagy controls Salmonella infection in response to damage to the Salmonella-containing vacuole. The Journal of biological chemistry 281, 11374-11383, doi:10.1074/jbc.M509157200 (2006).

2 Ogawa M, Y. T., Suzuki T, Sagara H, Mizushima N, Sasakawa C. Escape of Intracellular Shigella from Autophagy. Science 307, 727-731, doi:10.1126/science.1106036 (2005).

3 Knævelsrud, H. & Simonsen, A. Fighting disease by selective autophagy of aggregate-prone proteins. FEBS Letters 584, 2635-2645, doi:http://dx.doi.org/10.1016/j.febslet.2010.04.041 (2010).

4 Kondo, Y., Kanzawa, T., Sawaya, R. & Kondo, S. The role of autophagy in cancer development and response to therapy. Nat Rev Cancer 5, 726-734, doi:10.1038/nrc1692 (2005).

5 Shintani, T. & Klionsky, D. J. Autophagy in health and disease: a double-edged sword. Science 306, 990-995, doi:10.1126/science.1099993 (2004).

6 Finley, D. Recognition and processing of ubiquitin-protein conjugates by the proteasome. Annu Rev Biochem 78, 477-513, doi:10.1146/annurev.biochem.78.081507.101607 (2009).

7 Yang, Z. & Klionsky, D. J. An overview of the molecular mechanism of autophagy. Curr Top Microbiol Immunol 335, 1-32, doi:10.1007/978-3-642-00302-8_1 (2009).

8 Mijaljica, D., Prescott, M. & Devenish, R. J. Microautophagy in mammalian cells: Revisiting a 40-year-old conundrum. Autophagy 7, 673-682 (2011).

9 Li, W. W., Li, J. & Bao, J. K. Microautophagy: lesser-known self-eating. Cell Mol Life Sci 69, 1125-1136, doi:10.1007/s00018-011-0865-5 (2012).

10 Bejarano, E. & Cuervo, A. M. Chaperone-mediated autophagy. Proc Am Thorac Soc 7, 29-39, doi:10.1513/pats.200909-102JS (2010).

11 Mizushima, N. Autophagy: process and function. Genes Dev 21, 2861-2873, doi:10.1101/gad.1599207 (2007).

12 Mizushima, N., Yoshimori, T. & Ohsumi, Y. The Role of Atg Proteins in Autophagosome Formation. Annual Review of Cell and Developmental Biology, Vol 27 27, 107-132, doi:DOI 10.1146/annurev-cellbio-092910-154005 (2011).

13 Weidberg, H., Shvets, E. & Elazar, Z. Biogenesis and cargo selectivity of autophagosomes. Annu Rev Biochem 80, 125-156, doi:10.1146/annurev-biochem-052709-094552 (2011).

14 Klionsky, D. J. & Ohsumi, Y. Vacuolar import of proteins and organelles from the cytoplasm. Annu Rev Cell Dev Biol 15, 1-32, doi:10.1146/annurev.cellbio.15.1.1 (1999).

15 Baba, M., Takeshige, K., Baba, N. & Ohsumi, Y. Ultrastructural analysis of the autophagic process in yeast: detection of autophagosomes and their characterization. The Journal of cell biology 124, 903-913 (1994).

16 Kuma, A. et al. The role of autophagy during the early neonatal starvation period. Nature 432, 1032-1036, doi:10.1038/nature03029 (2004).

17 Fimia, G. M., Kroemer, G. & Piacentini, M. Molecular mechanisms of selective autophagy. Cell Death and Differentiation 20, 1-2, doi:Doi 10.1038/Cdd.2012.97 (2013).

18 Kamada, Y. et al. Tor directly controls the Atg1 kinase complex to regulate autophagy. Mol Cell Biol 30, 1049-1058, doi:10.1128/MCB.01344-09 (2010).

19 Kamada, Y. et al. Tor-mediated induction of autophagy via an Apg1 protein kinase complex. The Journal of cell biology 150, 1507-1513 (2000).

20 Klionsky, D. J. et al. A unified nomenclature for yeast autophagy-related genes. Developmental Cell 5, 539-545, doi:Doi 10.1016/S1534-5807(03)00296-X (2003).

21 Kabeya, Y. et al. Atg17 functions in cooperation with Atg1 and Atg13 in yeast autophagy. Mol Biol Cell 16, 2544-2553, doi:10.1091/mbc.E04-08-0669 (2005).

22 Cheong, H., Nair, U., Geng, J. & Klionsky, D. J. The Atg1 kinase complex is involved in the regulation of protein recruitment to initiate sequestering vesicle formation for nonspecific

autophagy in Saccharomyces cerevisiae. Mol Biol Cell 19, 668-681, doi:10.1091/mbc.E07-08-0826 (2008).
23 Mizushima, N. The role of the Atg1/ULK1 complex in autophagy regulation. Current opinion in cell biology 22, 132-139, doi:10.1016/j.ceb.2009.12.004 (2010).
24 Jaber, N. et al. Class III PI3K Vps34 plays an essential role in autophagy and in heart and liver function. Proceedings of the National Academy of Sciences of the United States of America 109, 2003-2008, doi:DOI 10.1073/pnas.1112848109 (2012).
25 Noda, T. et al. Apg9p/Cvt7p is an integral membrane protein required for transport vesicle formation in the Cvt and autophagy pathways. The Journal of cell biology 148, 465-480 (2000).
26 He, C. C. et al. Recruitment of Atg9 to the preautophagosomal structure by Atg11 is essential for selective autophagy in budding yeast. Journal of Cell Biology 175, 925-935, doi:DOI 10.1083/jcb.200606084 (2006).
27 Ichimura, Y. et al. A ubiquitin-like system mediates protein lipidation. Nature 408, 488-492 (2000).
28 Fujita, N. et al. The Atg16L complex specifies the site of LC3 lipidation for membrane biogenesis in autophagy. Molecular Biology of the Cell 19, 2092-2100, doi:DOI 10.1091/mbc.E07-12-1257 (2008).
29 Yamada, Y. et al. The crystal structure of Atg3, an autophagy-related ubiquitin carrier protein (E2) enzyme that mediates Atg8 lipidation. The Journal of biological chemistry 282, 8036-8043, doi:10.1074/jbc.M611473200 (2007).
30 Sou, Y. S. et al. The Atg8 conjugation system is indispensable for proper development of autophagic isolation membranes in mice. Mol Biol Cell 19, 4762-4775, doi:10.1091/mbc.E08-03-0309 (2008).
31 Stangler, T., Mayr, L. M. & Willbold, D. Solution structure of human GABA(A) receptor-associated protein GABARAP: implications for biolgoical funcrion and its regulation. The Journal of biological chemistry 277, 13363-13366, doi:10.1074/jbc.C200050200 (2002).
32 Coyle, J. E., Qamar, S., Rajashankar, K. R. & Nikolov, D. B. Structure of GABARAP in two conformations: implications for GABA(A) receptor localization and tubulin binding. Neuron 33, 63-74 (2002).
33 Bavro, V. N. et al. Crystal structure of the GABA(A)-receptor-associated protein, GABARAP. EMBO reports 3, 183-189, doi:10.1093/embo-reports/kvf026 (2002).
34 Knight, D. et al. The X-ray crystal structure and putative ligand-derived peptide binding properties of gamma-aminobutyric acid receptor type A receptor-associated protein. The Journal of biological chemistry 277, 5556-5561, doi:10.1074/jbc.M109753200 (2002).
35 Sugawara, K. et al. Crystallization and preliminary X-ray analysis of LC3-I. Acta Crystallogr D Biol Crystallogr 59, 1464-1465 (2003).
36 Noda, N. N. et al. Structural basis of target recognition by Atg8/LC3 during selective autophagy. Genes Cells 13, 1211-1218, doi:10.1111/j.1365-2443.2008.01238.x (2008).
37 Shintani, T. & Klionsky, D. J. Cargo proteins facilitate the formation of transport vesicles in the cytoplasm to vacuole targeting pathway. Journal of Biological Chemistry 279, 29889-29894, doi:DOI 10.1074/jbc.M404399200 (2004).
38 Lynch-Day, M. A. & Klionsky, D. J. The Cvt pathway as a model for selective autophagy. FEBS Lett 584, 1359-1366, doi:10.1016/j.febslet.2010.02.013 (2010).
39 Behrends, C. & Fulda, S. Receptor proteins in selective autophagy. International journal of cell biology 2012, 673290, doi:10.1155/2012/673290 (2012).
40 Cheung, Z. H. & Ip, N. Y. The emerging role of autophagy in Parkinson's disease. Molecular Brain 2, doi:Artn 29
Doi 10.1186/1756-6606-2-29 (2009).
41 Lynch-Day, M. A., Mao, K., Wang, K., Zhao, M. T. & Klionsky, D. J. The Role of Autophagy in Parkinson's Disease. Cold Spring Harbor Perspectives in Medicine 2, doi:ARTN a009357
DOI 10.1101/cshperspect.a009357 (2012).
42 Ling, D. & Salvaterra, P. M. A central role for autophagy in Alzheimer-type neurodegeneration. Autophagy 5, 738-740 (2009).

43 Kanki, T., Wang, K., Cao, Y., Baba, M. & Klionsky, D. J. Atg32 is a mitochondrial protein that confers selectivity during mitophagy. Dev Cell 17, 98-109, doi:10.1016/j.devcel.2009.06.014 (2009).

44 Hutchins, M. U., Veenhuis, M. & Klionsky, D. J. Peroxisome degradation in Saccharomyces cerevisiae is dependent on machinery of macroautophagy and the Cvt pathway. Journal of Cell Science 112, 4079-4087 (1999).

45 Dunn, W. A. et al. Pexophagy - The selective autophagy of peroxisomes. Autophagy 1, 75-83 (2005).

46 Graef, M., Friedman, J. R., Graham, C., Babu, M. & Nunnari, J. ER exit sites are physical and functional core autophagosome biogenesis components. Mol Biol Cell 24, 2918-2931, doi:10.1091/mbc.E13-07-0381 (2013).

47 Krick, R. et al. Piecemeal Microautophagy of the Nucleus Requires the Core Macroautophagy Genes. Molecular Biology of the Cell 19, 4492-4505, doi:DOI 10.1091/mbc.E08-04-0363 (2008).

48 Buchan, J. R., Kolaitis, R. M., Taylor, J. P. & Parker, R. Eukaryotic Stress Granules Are Cleared by Autophagy and Cdc48/VCP Function. Cell 153, 1461-1474, doi:DOI 10.1016/j.cell.2013.05.037 (2013).

49 Yuga, M., Gomi, K., Klionsky, D. J. & Shintani, T. Aspartyl aminopeptidase is imported from the cytoplasm to the vacuole by selective autophagy in Saccharomyces cerevisiae. The Journal of biological chemistry 286, 13704-13713, doi:10.1074/jbc.M110.173906 (2011).

50 Suzuki, K., Morimoto, M., Kondo, C. & Ohsumi, Y. Selective autophagy regulates insertional mutagenesis by the Ty1 retrotransposon in Saccharomyces cerevisiae. Dev Cell 21, 358-365, doi:10.1016/j.devcel.2011.06.023 (2011).

51 Suzuki, K., Kondo, C., Morimoto, M. & Ohsumi, Y. Selective transport of alpha-mannosidase by autophagic pathways: identification of a novel receptor, Atg34p. The Journal of biological chemistry 285, 30019-30025, doi:10.1074/jbc.M110.143511 (2010).

52 Watanabe, Y. et al. Selective transport of alpha-mannosidase by autophagic pathways: structural basis for cargo recognition by Atg19 and Atg34. The Journal of biological chemistry 285, 30026-30033, doi:10.1074/jbc.M110.143545 (2010).

53 Kim, J., Huang, W. P., Stromhaug, P. E. & Klionsky, D. J. Convergence of multiple autophagy and cytoplasm to vacuole targeting components to a perivacuolar membrane compartment prior to de novo vesicle formation. The Journal of biological chemistry 277, 763-773, doi:10.1074/jbc.M109134200 (2002).

54 Yorimitsu, T. & Klionsky, D. J. Atg11 links cargo to the vesicle-forming machinery in the cytoplasm to vacuole targeting pathway. Mol Biol Cell 16, 1593-1605, doi:10.1091/mbc.E04-11-1035 (2005).

55 Chang, C. Y. & Huang, W. P. Atg19 mediates a dual interaction cargo sorting mechanism in selective autophagy. Mol Biol Cell 18, 919-929, doi:10.1091/mbc.E06-08-0683 (2007).

56 Umekawa, M. & Klionsky, D. J. The Cytoplasm-to-Vacuole Targeting Pathway: A Historical Perspective. International journal of cell biology 2012, 142634, doi:10.1155/2012/142634 (2012).

57 Morales Quinones, M., Winston, J. T. & Stromhaug, P. E. Propeptide of aminopeptidase 1 protein mediates aggregation and vesicle formation in cytoplasm-to-vacuole targeting pathway. The Journal of biological chemistry 287, 10121-10133, doi:10.1074/jbc.M111.311696 (2012).

58 Kim, J., Scott, S. V., Oda, M. N. & Klionsky, D. J. Transport of a large oligomeric protein by the cytoplasm to vacuole protein targeting pathway. The Journal of cell biology 137, 609-618 (1997).

59 Shintani, T., Huang, W. P., Stromhaug, P. E. & Klionsky, D. J. Mechanism of cargo selection in the cytoplasm to vacuole targeting pathway. Dev Cell 3, 825-837 (2002).

60 Scott, S. V., Guan, J., Hutchins, M. U., Kim, J. & Klionsky, D. J. Cvt19 is a receptor for the cytoplasm-to-vacuole targeting pathway. Mol Cell 7, 1131-1141 (2001).

61 Noda, N. N., Ohsumi, Y. & Inagaki, F. Atg8-family interacting motif crucial for selective autophagy. FEBS Lett 584, 1379-1385, doi:10.1016/j.febslet.2010.01.018 (2010).

62 Pankiv, S. et al. p62/SQSTM1 binds directly to Atg8/LC3 to facilitate degradation of ubiquitinated protein aggregates by autophagy. The Journal of biological chemistry 282, 24131-24145, doi:10.1074/jbc.M702824200 (2007).
63 Wild, P. et al. Phosphorylation of the autophagy receptor optineurin restricts Salmonella growth. Science 333, 228-233, doi:10.1126/science.1205405 (2011).
64 von Muhlinen, N. et al. LC3C, bound selectively by a noncanonical LIR motif in NDP52, is required for antibacterial autophagy. Mol Cell 48, 329-342, doi:10.1016/j.molcel.2012.08.024 (2012).
65 Gibbings, D. et al. Selective autophagy degrades DICER and AGO2 and regulates miRNA activity. Nat Cell Biol 14, 1314-1321, doi:10.1038/ncb2611 (2012).
66 von Muhlinen, N., Thurston, T., Ryzhakov, G., Bloor, S. & Randow, F. NDP52, a novel autophagy receptor for ubiquitin-decorated cytosolic bacteria. Autophagy 6, 288-289 (2010).
67 <J. Biol. Chem.-2012-Morales Quinones_Propeptide of Aminopeptidase 1 Protein Mediates.pdf>.
68 Alemu, E. A. et al. ATG8 family proteins act as scaffolds for assembly of the ULK complex: sequence requirements for LC3-interacting region (LIR) motifs. The Journal of biological chemistry 287, 39275-39290, doi:10.1074/jbc.M112.378109 (2012).

Abbreviations

ABD	Ams1-binding domain
Ams1	α-mannosidase 1
Atg	Autophagyrelatedgeneproduct
CBB	Coomassie Brilliant Blue
cc	coiled-coil
CMA	Chaperone-mediatedautophagy
Cvt	Cytoplasm-to-vacuole-targeting
DGS-NTA	(1,2-dioleoyl-*sn*-glycero-3-[(N-(5-aminocarboxypentyl)iminodiaceticacid) succinyl] (nickelsalt)
DTT	dithiotreitol
EtOH	Ethanole
Fig.	Figure
GSH	glutathione
GST	glutathione-S-Transferase
His	Histidin
IPTG	Isopropyl β-D-1-thiogalactopyranoside
kD	Kilo Daltons
LIR	LC3-interacting region
PAGE	polyacrylamidgelelectrophoresis
PE	Phosphatidyl-ethanolamine
PI3P	Phosphatidyl-inositol-3-phosphate
POPC	Phosphatidyl-choline
prApe1	precursorof vacuolar aminopeptidase 1
SDS	Sodium-dodecyl-sulfate
SEC	Size exclusionchromatography
TBS(T)	Tris-buffered saline (containing 0.1% Tween 100)
TOR	Target-of-rapamycine

Vienna, November 28 2013

Curriculum Vitae

Name:	Christine Isabel Abert
Studies:	October 2008-Juli 2011 Bachelorstudies of Biology at LMU München, Bachelorarbeit in Prof. Jürgen Soll's group (plant biochemistry) since October 2011 Master studies of Molecular Biology at the University of Vienna

Acknowledgements

I would like to thank several people who greatly helped me during the work on this thesis. Dr. Sascha Martens gave me the unique opportunity to work in his group on this highly interesting project. As a supervisor, he has always been very supportive, open-minded, enthusiastic and patient to answer any kind of questions and to explain various laboratory techniques. I am also very grateful to Dr. Justyna Sawa-Makarska for being a wonderful teacher. She was never tired to give insightful advice, explanations or ideas on experiments and results and created a great mood in the lab. Julia Romanov, Marta Walczak and Bettina Wurzer showed me how to conduct several experiments or shared priceless tipps and tricks with me. Dorotea Fracchiolla, Gabriele Zaffagnini and Bettina Zens never hesitated to discuss any lab or science related questions. I am thankful to Dr. Claudine Kraft and her group for helping out with equipment and always being open for questions and discussions. I very much appreciated the friendly, open and yet very professional working atmosphere in the lab(s) and I think I have really gained a lot of theoretical and practical knowledge in these past one and a half years. I am grateful to Dr. Tim Clausen and his group for letting me conduct experiments on their HPLC and on their ITC systems, to Prof. Kristina Djinovic and her group for letting me use their SLS system, to Prof. Robert Konrat and his group for helping me conducting NMR experiments.

Another Thank you goes to my parents and my sister Julia for their great support and helpfulness. Thanks a lot to Sabrina for giving me very useful advice and to Mireille and the whole WG for maintaining our cozy spot in Vienna. Thank you to Gerard for providing me with essential software and teaching me the handling and language thereof.

Hiermit versichere ich, Christine Abert, die vorliegende Masterarbeit zum Thema „Mechanisms of Cargo Selection in Cytoplasm-To-Vacuole-Targeting“ selbständig verfasst zu haben und ausschließlich die angegebenen Quellen und Hilfsmittel verwendet sowie Gedanken und Formulierungen aus diesen in angemessener Form gekennzeichnet zu haben.

Wien, den 04.12.2013